



Synthesis and antiproliferative activity of 6BrCaQ-TPP conjugates for targeting the mitochondrial heat shock protein TRAP1

Clelia Mathieu, Quentin Chamayou, Thi Thanh Hyen Luong, Delphine Naud, Florence Mahuteau-Betzer, Mouad Alami, Elias Fattal, Samir Messaoudi, Juliette Vergnaud-Gauduchon

► To cite this version:

Clelia Mathieu, Quentin Chamayou, Thi Thanh Hyen Luong, Delphine Naud, Florence Mahuteau-Betzer, et al.. Synthesis and antiproliferative activity of 6BrCaQ-TPP conjugates for targeting the mitochondrial heat shock protein TRAP1. *European Journal of Medicinal Chemistry*, 2022, 229, pp.114052. 10.1016/j.ejmech.2021.114052 . hal-03795373

HAL Id: hal-03795373

<https://hal.science/hal-03795373>

Submitted on 8 Jan 2024

HAL is a multi-disciplinary open access archive for the deposit and dissemination of scientific research documents, whether they are published or not. The documents may come from teaching and research institutions in France or abroad, or from public or private research centers.

L'archive ouverte pluridisciplinaire **HAL**, est destinée au dépôt et à la diffusion de documents scientifiques de niveau recherche, publiés ou non, émanant des établissements d'enseignement et de recherche français ou étrangers, des laboratoires publics ou privés.



Distributed under a Creative Commons Attribution - NonCommercial 4.0 International License

Synthesis and Antiproliferative Activity of 6BrCaQ-TPP conjugates for Targeting the Mitochondrial Heat Shock Protein TRAP1

Clelia Mathieu^[a], Quentin Chamayou^[b], Thi Thanh Hyen Luong^[b], Delphine Naud,^[c,d] Florence Mahuteau,^[c,d] Mouad Alami^[b], Elias Fattal^[a], Samir Messaoudi^{*[b]}, Juliette Vergnaud-Gauduchon^{*[a]}

^a Université Paris-Saclay, CNRS, Institut Galien-Paris Saclay, 92296 Châtenay-Malabry, France.

^b Université Paris-Saclay, CNRS, BioCIS, 92290 Châtenay, Malabry, France

^c Institut Curie, Université PSL, CNRS UMR9187, Inserm U1196, Chemistry and Modeling for the Biology of Cancer, 91400, Orsay, France

^d Université Paris-Saclay, CNRS UMR9187, Inserm U1196, Chemistry and Modeling for the Biology of Cancer, 91400, Orsay, France

Abstract

A series of 6BrCaQ-C_n-TPP conjugates **3a-f** and **5** was designed and synthesized as a novel class of TRAP1 inhibitors. Compound **3a** displayed an excellent anti-proliferative activity with mean GI₅₀ values at a nanomolar level in a diverse set of human cancer cells (GI₅₀ = 0.008-0.30 μM) including MDA-MB231, HT-29, HCT-116, K562, and PC-3 cancer cell lines. Moreover, the best lead compound 6BrCaQ-C₁₀-TPP induces a significant mitochondrial membrane disturbance combined to a regulation of HSP and partner protein levels as a first evidence that his mechanism of action involves the TRAP-1 mitochondrial Hsp90 machinery.

Keywords: TRAP1, 6BrCaQ, HSP90, triphenylphosphonium TPP, mitochondrial targeting, anti-proliferative activity.

1. Introduction

Heat-shock proteins (HSP) are involved in the homeostasis of healthy cells through their chaperoning activity (folding and maturation of proteins)¹. HSP90, especially, represents a family of chaperones assisting several client proteins, growth factor receptors, hormone receptors, signaling proteins, many of them involved in the hallmark of cancers². HSP90 appears therefore as an interesting new therapeutic target to overcome drug resistance^{3,4}. Four HSP90 isoforms have been identified; HSP90 α/β are mainly located in the cytosol, whereas TRAP1 (Tumour Necrosis Factor Receptor-associated Protein 1) and GRP94 are mostly located in the mitochondria and the endoplasmic reticulum, respectively. They mainly function as homodimers with the help of other HSP family members and co-chaperones. Many research groups focused their research on the inhibition of HSP90 through the modulation of its ATPase activity⁵. Different families of inhibitors, which act mainly on the N-terminal or the C-terminal domain, can target Hsp90. In short, the N-terminal domain is responsible for ATP binding and regulates the chaperone activity, a middle domain that helps the ATPase site (ATP hydrolysis) and binds client proteins, and finally a C-terminal domain involved in dimerization. Lots of N-terminal inhibitors went into clinical trials, based on four scaffolds: ansamycin (17-AAG, geldamycin, 17-DMAG, ...), resorcinol (radicol, NVP-AUY922, ...), purine, and benzamide^{5,6}. However, none of them is FDA-approved mainly because of an adverse response called Heat-Shock Response (HSR). HSR is characterized by the release of the transcription factor Heat Shock Factor-1 (HSF-1) from HSP90 chaperoning after the inhibitor binding and the subsequent induction of the transcription of the genes coding HSP90, HSP70, and HSP27 leading to an increased protein expression⁷.

Therefore, several groups focused their drug discovery research on inhibiting the C-terminal domain since it does not induce the release HSF-1. Several natural compounds, such as novobiocin and deguelin, displayed an inhibition activity on the C-terminal domain of HSP90. Structure-activity relationship studies allowed several groups to identify promising inhibitors with a mechanism of action distinct from N-terminal inhibitors⁸⁻¹². In this context, our group identified a very promising C-terminal HSP90 inhibitor named 6-BrCaQ. This compound was active on various cancer cell lines with a LC₅₀ of 5-50 μM ¹³⁻¹⁶. It induced apoptosis and decreased the levels of client proteins of HSP90 on prostate cancer cells, PC3. Encapsulated in liposomes, 6BrCaQ exerted an improved *in vitro* activity on breast cancer cells (MDA-MB-231) and had an anti-tumor effect on an orthotopic breast cancer model in nude mice¹³.

Nevertheless, the toxicity attributed to HSP90 inhibitors can be explained by the lack of selectivity toward different isoforms. Thus, the second strategy is to develop selective inhibitors toward one isoform or able to reach only one intracellular compartment. Some research groups concentrated their work on GRP94 inhibition by modifying the structures of known inhibitors to make them more specific to GRP94¹⁷. The strategy was to attach rigid resorcinyl moieties to the scaffold resorcinyl benzyl imidazole that exhibits high selectivity for Grp94. Park *et al.*¹⁸ applied a similar strategy for TRAP1, by modifying the imidazole ring of a purine scaffold to bind the specific region of TRAP-1 identified on the crystal structure. However, the main strategy to target TRAP-1 remains adding a moiety targeting the mitochondria to the HSP90 inhibitor.

In cancer cells, mitochondria are major regulators of bioenergetics and apoptosis. Targeting the mitochondria has recently emerged as a good strategy for cancer treatment. They mediate one of the signaling of apoptosis through regulation of ATP synthesis, cytochrome c release, and ROS (Reactive Oxygen Species) production^{19,20}. Furthermore, mitochondria are involved in the metabolic rewiring during the malignant process. Several mechanisms are altered : the

glucose metabolism and oxidative phosphorylation (OXPHOS) independently of the oxygen availability (Warburg effect), the accumulation of mitochondrial metabolites to fulfill anabolic need, and the function of the mitochondrial permeability transition port (mPTP). TRAP1 expression is restricted to mitochondria and only few client proteins are identified. But TRAP1 has protective functions towards mitochondria through the inhibition of Succinate dehydrogenase (SDH) and **downregulation of the complex IV of the respiratory chain, both mechanisms inducing invasiveness of tumor cells and metabolic rewiring. TRAP1 has also been shown to negatively control the mPTP.**

Over the years, among the molecules that can be used to reach targeting of mitochondria, many are lipophilic cations, able to accumulate within mitochondria because of a greater potential difference across the mitochondrial membrane (highly negative) compared to the plasma membrane. Among the promising targeting moieties the dequalinium, guanidinium, triethylammonium, pyridinium, 3-phenylsulfonylfuroxan, 2,3-dimethylbenzothiazolium iodide, rhodamine, cationic peptides, and triphenylphosphonium (TPP⁺) have shown mitochondrial selectivity²¹. This last one has notably been used to bring dye and image enhancers or drugs into mitochondria, like MitoQ^{22,23}.

By combining the N-terminal HSP90 inhibitor (17-AAG) with various linkers' lengths and a mitochondrial targeting moiety as TPP⁺ and guanidinium salts²⁴, Kang *et al.* developed gamitrinibs to inhibit TRAP1. The authors showed that a long chain (aliphatic) increases mitochondrial accumulation. The targeted inhibitor derived from 17-AAG was 6 to 10 times more potent than the untargeted one depending on cell lines, confirming the rationale to target mitochondria to enhance the activity of HSP90 inhibitors. The same group combined a specific inhibitor of TRAP1 (with a 3,4-isoxazole diamide, N-terminal inhibitor²⁵) to a mitochondrial delivery vehicle. In the same way, they varied the linker length and the cationic head (TPP⁺ or guanidinium) and they obtained similar binding affinities (in the nmol/L range) toward HSP90 and TRAP1. However, they showed an accumulation into the mitochondria, associated with a good ATPase inhibition (IC₅₀ around 0.5 μmol/L). Cell proliferation was inhibited (IC₅₀ = 1.32 μmol/L) and cells underwent apoptosis starting at 1 μmol/L. Thomas *et al.* combined as a triple conjugate a pyridinium ion for mitochondrial targeting, a purine derivative for N-terminal TRAP1 inhibition, and a photosensitizer for photodynamic therapy. Interestingly, they showed a co-localization of this compound with the mitochondria stained by mitotracker green® in HeLa, NCI-H460 cancer cells but not in normal hepatocytes²⁶.

Since N-terminal inhibitors present limitations such as the HSR, it would be interesting to combine the mitochondrial targeting property to selectively inhibit TRAP1 in the C-terminal domain. Herein, we succeeded in combining both strategies by modifying the previously synthesized HSP90 C-terminal inhibitor 6BrCaQ. To target the mitochondria a triphenylphosphonium ion will be added through various linkers (Figure 1). To this end, the synthetic strategy will be based on two selective nucleophilic substitutions of the di-bromoalkane linkers with two different nucleophiles: the phenol of 6BrCaQ from one side and the triphenylphosphine from another side (Figure 1). The length of the linker will be modified to better understand the SAR in this novel series. In this article, the synthesis and the biological evaluation of novel 6BrCaQ-C_n-TPP analogues **3a-f** and **5** are described. Preliminary *in vitro* efficacy of these compounds in terms of antiproliferative effect is reported. The selected best analogue 6BrCaQ-C₁₀-TPP has been tested *in vitro* in a colon cancer model (HT29) for proliferation, mitochondrial disruption, and expression of TRAP1 partners demonstrating promising properties of inhibition of TRAP1. **To** the best of our knowledge, never has such an approach for targeting TRAP by using C-terminal inhibitors been reported.

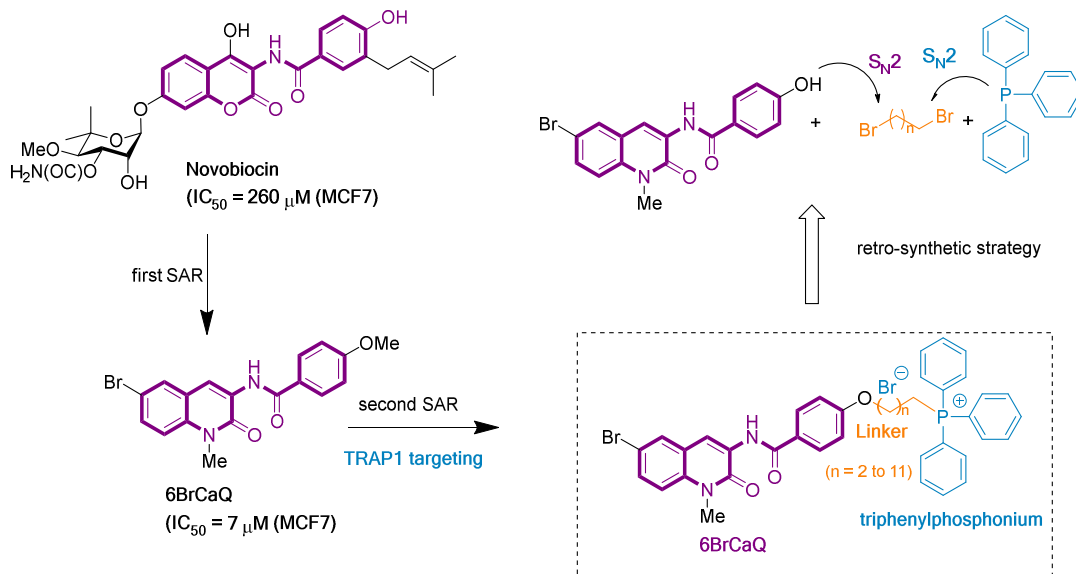


Figure 1. Structures of novobiocin, synthetic derivative 6BrCaQ and targeted 6BrCaQ-C_n-TPP derivatives.

2. Results and discussion

2.1. Chemistry.

The synthesis of the target 6BrCaQ-TPP conjugates **3a-f** and **5** is summarized in Scheme 1. *p*-hydroxyl benzamide quinolinones **1a** and **1b** were prepared first as it was previously reported¹⁵ by selective coupling of the di-bromoquinolinone with *p*-hydroxyl benzamide under Pd-catalysis. Compounds **1a** and **1b** were obtained in 90% yield. With a gram scale amount of **1a** in hand, we envisioned at first the synthesis of the 6BrCaQ-C10-TPP analogue. To this end, reaction of **1a** with a large excess of 1,10 dibromodecane (8 to 10 equiv.) in the presence of potassium carbonate at the reflux of acetone furnished selectively the mono-alkylated compound **2a** in 76% yield (Scheme 1, path A). The final step evolves the nucleophilic substitution of the second C-Br bond by the triphenylphosphine to produce the 6BrCaQ-C10-TPP (compound **3a**) in 50% yield.

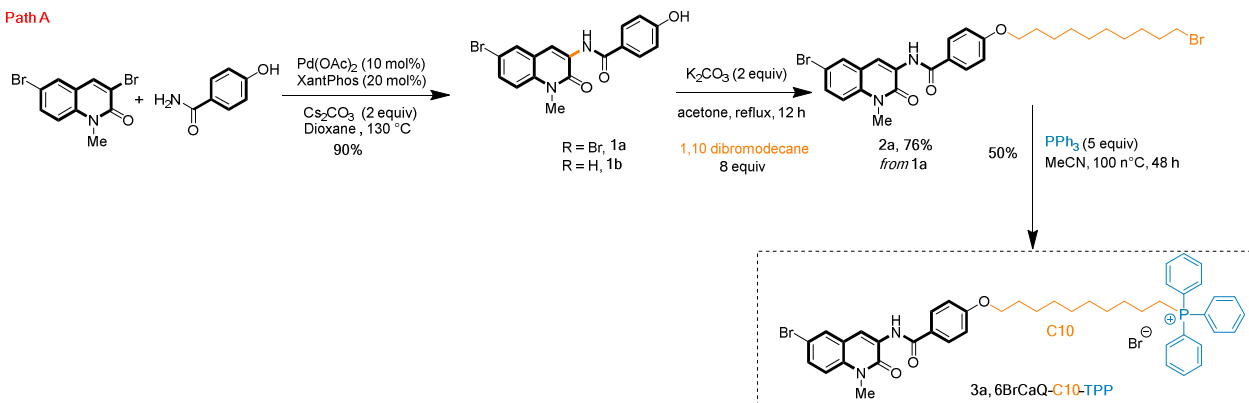
In another strategy, the possibility of a fast and easy access to a series of 6BrCaQ-C₁₀-TPP analogues in which the length of the linker is modified was explored. As bromoalkylphosphoniums **4** bearing different lengths are commercially available, we decided to perform the nucleophilic substitution of **1a,b** with a selected series of bromoalkylphosphoniums (1.2 equiv) under basic conditions (K₂CO₃, DMF, 60 °C, 2 h, Scheme 1, path B). By this new approach which involves only one step without the need of using any large excess of starting materials, a series of 6BrCaQ-C_n-TPP analogues **3a-f** and **5** were successfully prepared in variable yields. Short linker lengths ranging between C3 and C7 (compounds **3b-e**, Scheme 1) could be introduced instead of the C10 reference. In addition, the compound **3f** bearing a C12 carbon length (6BrCaQ-C₁₂-TPP) was prepared. Finally, to examine the importance of the C-Br bond on the biological activity, analogue **5** lacking the Br atom (CaQ-C₁₀-TPP) was synthesized through this strategy starting from the intermediate **1b**.

1

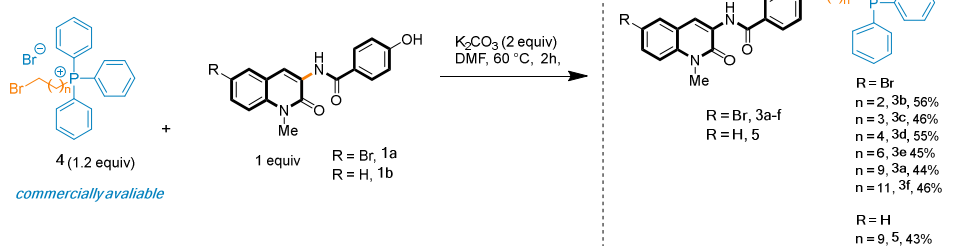
2

Scheme 1. Synthesis of compounds **3a-f** and **5**.

Path A



Path B



3

4

2.2. In vitro biological evaluation on cancer cells

5

2.2.1. Cytotoxicity

6

7

8

9

10

11

12

13

14

15

16

17

18

19

20

21

22

Upon completion of their syntheses, the *in vitro* activity of 6BrCaQ-TPP conjugates **3-f** and **5** was evaluated by their growth-inhibitory potency in MDA-MB-231 cancer cell line. The quantification of cell survival was established by using CellTiter Glo (Promega) assay after 72 h exposure (Figure 2A), and GI_{50} , TGI, LC_{50} et IC_{50} values were determined for each compound. The “hit” analogue was chosen according to the GI_{50} , IC_{50} (dose that induces 50 percent of the maximum inhibitory effect), and to the LC_{50} (dose that induces 50 percent of cell death). All the compounds displayed a high inhibitory effect with IC_{50} ranging between 0.008 and 0.082 μM , except for compound **3f** bearing the longest linker length (C12, GI_{50} of 11 μM). This first result demonstrates clearly that the conjugation of the Hsp90 C-terminus inhibitor with the phosphonium head increased significantly the biological activity toward the MDA-MB-231 cell line compared to the reference compound 6BrCaQ (IC_{50} = 0.9 μM) and 6BrCaQ-OH (**2a**) (IC_{50} = 7 μM). Interestingly, compound **5** which lacks the C-Br bond at the C7 position of the quinolinone nucleus displays a good activity as compared to the brominated different analogues with an IC_{50} = 0.049 μM and an LC_{50} = 0.31 μM . It appeared during this study that the C10-linked analogue **3a** (6BrCaQ-C10-TPP) showed the most promising activity (GI_{50} = IC_{50} = 0.008 μM and LC_{50} of 0.18 μM) (Figure 1B). As reported, the efficacy of the mitochondrial targeting depends on the lipophilicity of the cation, and thus of the linker. Indeed, the more lipophilic the molecule is, the faster the uptake is²². For example, it has been shown in Jurkat cells, that the uptake of decyl-triphenylphosphonium was faster (30 minutes) than the uptake of triphenylmethyl phosphonium (between 6 h and 8 h)²⁷. In addition, our result is consistent with another study related to the conjugation of metformin with the triphenylphosphonium²⁸. In this study,

the authors varied the length of the alkyl linker from C2 to C12 carbons and showed similarly to us that, the more efficient conjugate was the one with the decyl linker²⁸.

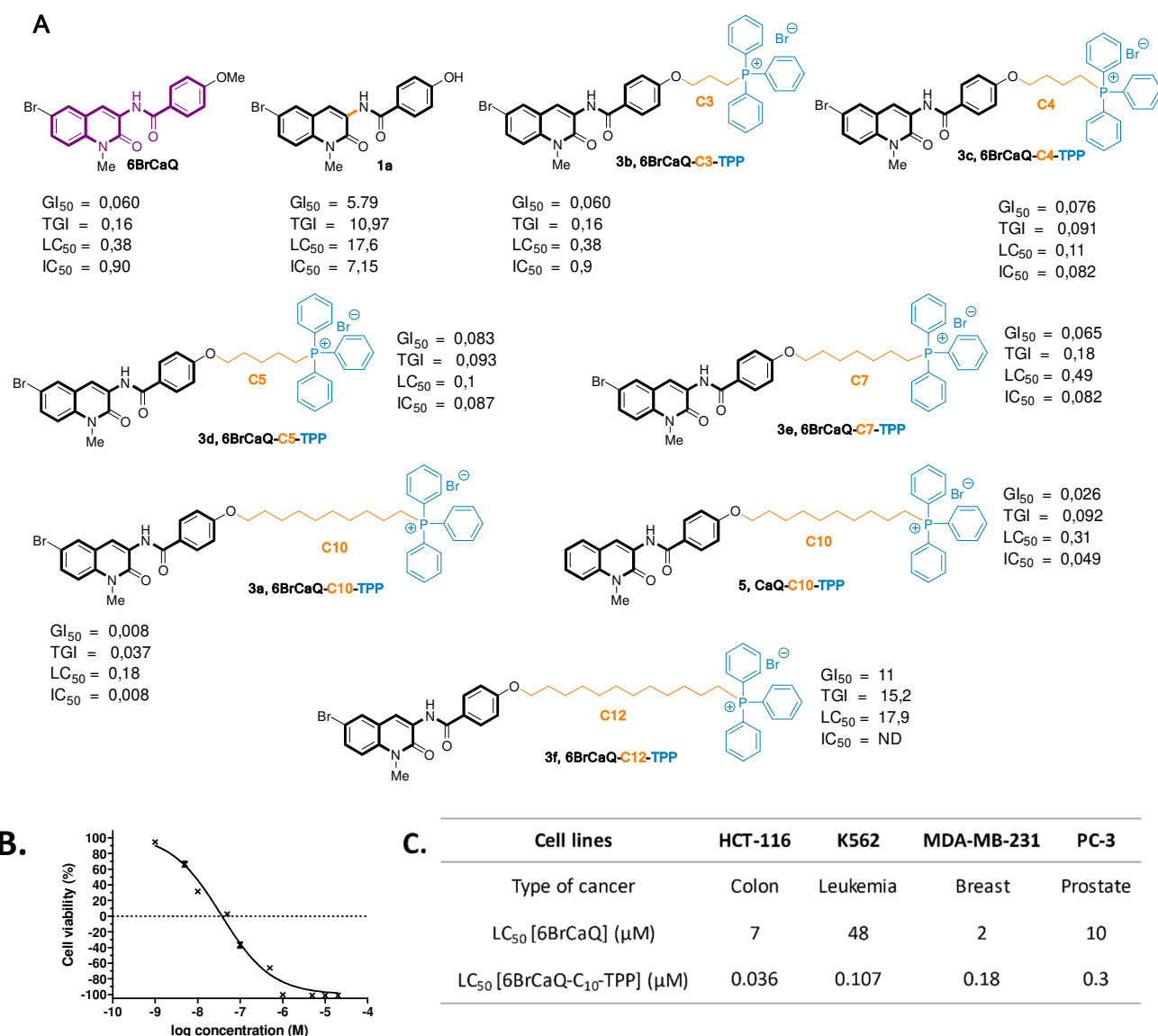


Figure 2. A. Value of GI₅₀, TGI₅₀, LC₅₀, IC₅₀ (μM) of 6BrCaQ, **1a**, compounds **3a-f** and **5** against MDA-MB-231 cancer cell lines measured by the CellTiter Glo (Promega). **(B)** IC₅₀ (μM) curve of 6BrCaQ-C₁₀-TPP against MDA-MB-231 cell lines **(C)** IC₅₀ against several cell lines treated by 6BrCaQ and 6BrCaQ-C₁₀-TPP measured by MTT at 72h. **GI₅₀**: the concentration that gives 50 % growth inhibition, often also referred to as IC₅₀, **TGI** (the concentration that gives a total growth inhibition meaning that the number of cells at the end of the exposure is similar to that at the beginning), **LC₅₀** (the concentration that gives 50 % cell kill, meaning that at the end the number of cells is 50 % of the number of cells at the beginning), **IC₅₀**: the concentration at which cell activity is inhibited by 50%.

This enhanced activity is further corroborated by the results obtained with gamitrinib. The addition of the targeting moiety on 17-AAG (TPP⁺ and others) lowered the IC₅₀²⁴. This study also showed a decrease of the mitochondrial potential upon uptake of the mitochondrial-targeted molecules, measured by TMRM. Moreover, another study showed that the gamitrinib linked with a TPP⁺ moiety also induced a depolarization of the mitochondria (measured by JC-1)³⁰. This altered mitochondrial potential can be caused by two factors: the mitochondrial-targeted moiety (TPP⁺) or the

HPS90 inhibition moiety (6BrCaQ). Indeed, the positively charged triphenylphosphonium can decrease by itself the mitochondrial membrane potential as shown by Lyamzaev *et al.* who used with a dodecyl triphenylphosphonium and a TMRM staining for detection³¹. That observation is consistent with the decrease induced by TPP-C₁₀-OH we observed at 3 and 6 h (See below, Figure 5). The inhibition of TRAP1 in itself can cause depolarization of the mitochondria. For instance, the neutral TRAP1 inhibitor (DN401) developed by Park *et al.*, is also decreasing the mitochondrial potential (measured by JC-1) by changing the metabolism of the cells induced by the inhibition of the TRAP1 machinery¹⁸. This double effect can explain the enhanced effect of 6BrCaQ-C₁₀-TPP compared to TPP-C₁₀-OH. Another explanation could be the difference in membrane permeability between the two molecules affecting their intracellular concentrations.

2.2.2 Antiproliferative activity

With the selected best analogue 6BrCaQ-C₁₀-TPP in hand, further anti-proliferative assays were performed on different types of cancer cells after 72 h of treatment (Figure 1C): HCT-116 (colon cancer), K562 (leukemia), MDA-MB-231 (breast cancer), and PC-3 (prostate cancer). The activity of 6BrCaQ-C₁₀-TPP was then compared to the activity of 6BrCaQ published previously¹⁴. Even if the IC₅₀ of 6BrCaQ on MDA-MB-231 cell lines was measured by MTT whereas the one of PC-3 was measured by MTS, both after 72 h of treatment, the 6BrCaQ-C₁₀-TPP was from 20 to 500-fold more efficient than the 6BrCaQ on those cell lines. The mitochondria-targeted inhibitor was then more efficient than the non-targeted one.

Further experiments were undertaken to decipher the mechanism of action of the selected 6BrCaQ-C₁₀-TPP. All future experiments will be focused on only one cell line: the colon cancer cell line HT-29.

As shown in Figure 3, the cytotoxic effect and the anti-proliferative effect of 6-BrCaQ-C₁₀-TPP was checked in HT-29 cell line. First, the metabolic activity was tested by MTT after 72 h of treatment: 6-BrCaQ-C₁₀-TPP displayed an IC₅₀ slightly lower than 0.1 μ M that is an improvement over 200-fold compared to 6-BrCaQ (Figure 3A). However, MTT, as well as other metabolic assays (MTS, ATPlite...), can be influenced when the mitochondrial metabolism of the cell is modified³². Thus, to confirm the cytotoxicity of our lead compound, alive and dead cells were counted after Trypan Blue exclusion upon 72 h of treatment. The results, shown in Figure 3B, are coherent with an anti-proliferative effect associated with few dead cells counted (no more than 10% compared to the total number of cells in control wells). The IC₅₀ calculated in the Trypan blue experiment is slightly lower than 0.1 μ M.

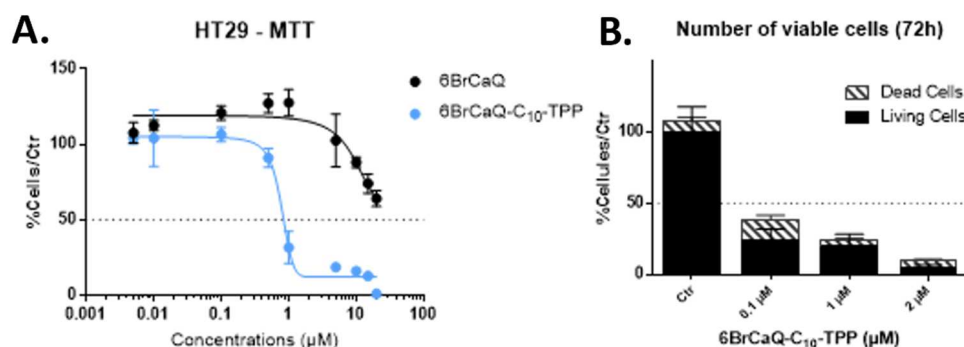


Figure 3. Anti-Proliferative effect and cell death induced by 6BrCaQ-C₁₀-TPP on HT29 cells. **A.** HT29 cells were treated by 6BrCaQ-C₁₀-TPP or 6BrCaQ for 72 h and analyzed by MTT. The mitochondrial targeting lowered significantly the IC₅₀ of the inhibitor. The graph is representative of 3 experiments. **B.** HT29 cells were treated by

6BrCaQ-C₁₀-TPP for 72 h and alive and dead cells counted by Trypan blue exclusion. Small number of dead cells were counted, n=3.

The MTT on HT-29 cells corroborates our previous results: the IC₅₀ of 6BrCaQ is superior to 20 µM, previously published with an IC₅₀ of 32 µM¹⁵, and the targeting moiety to mitochondria enhanced the activity of the inhibitor with a 300-fold ratio, as in the other cell lines. To confirm the MTT assay, the Trypan blue dye exclusion counting confirmed the IC₅₀ on HT-29 cell lines. However it shows few dead cells, so it seems that the main effect is cell proliferation inhibition over apoptosis induction. It is in agreement with studies on the silencing of TRAP1^{33–35}. They showed that the knockdown of TRAP1 in different breast and colon cancer cells induced a reduction of cell growth. Agoretta *et al.* and Condelli *et al.* showed decrease of the S-phase, and a G₀-G₁ phase arrest, and in G₂-M phase. Whereas Palladino *et al.* showed a reduction of cells in G₂-M phase. Nonetheless, they all lead to the inhibition of the proliferation, supporting our results. The untargeted inhibitor 6BrCaQ induced a cycle arrest in G₂/M, and thus inhibiting the cell proliferation of PC-3 and MDA-MB-231 cells¹³.

2.2.3 Targeting of the mitochondria

To confirm the accumulation of 6-BrCaQ-C₁₀-TPP into mitochondria, the variation/disruption of mitochondrial membrane potential was evaluated. Indeed, this parameter is crucial for the function of mitochondria: it drives anions outward as well as cations inward transport, ATP synthesis (proton gradient) and the quality control system. Attenuation of this potential is a sign of early apoptosis, of the opening of the membrane permeability transport pore, of a change of ATP synthesis rate, or more importantly of an accumulation of lipophilic cations, as our inhibitor³⁶. To measure this potential, TMRE staining was used as shown in Figure 4A. According to the manufacturer's advice, microplate-fluorescence was preferred over flow cytometry as HT-29-cells are adherent cells and can't be scraped without altering cells, and as the staining is not compatible with trypsinization.

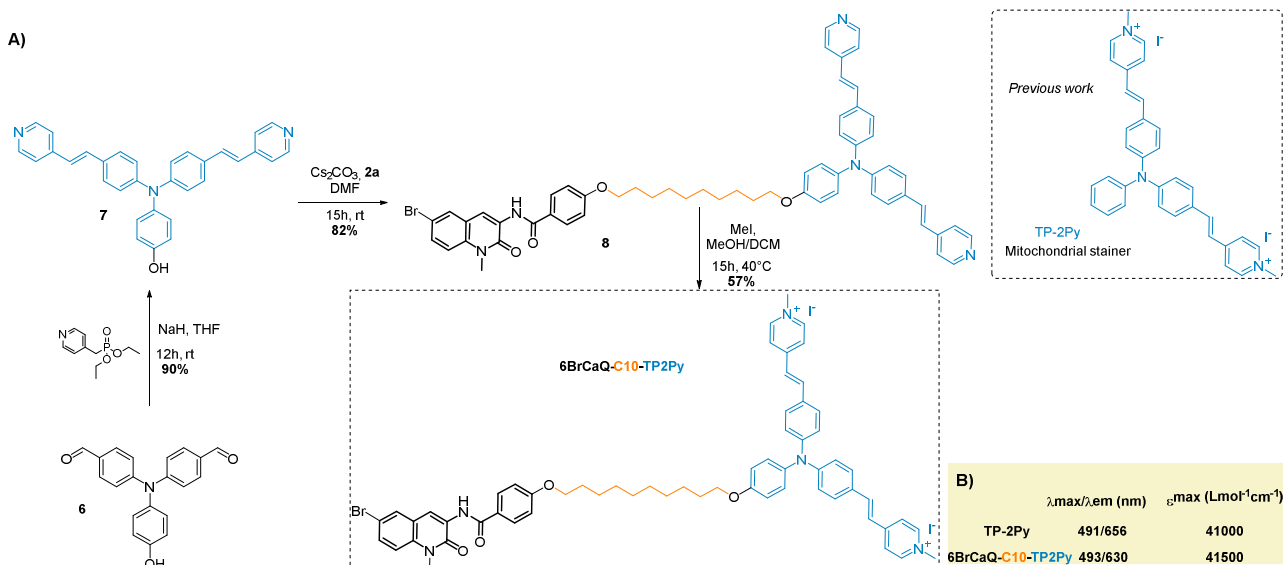
The mitochondrial membrane potential was measured at early time points: 2, 3, or 6 h at several doses (0.1, 0.5 and 1 µM) with three compounds: 6BrCaQ-C₁₀-TPP, TPP-C₁₀-OH, and 6BrCaQ (with an additional concentration of 5 µM) (Figure 5A). CCCP was used as a positive control of membrane potential disruption as it is an uncoupler of the mitochondrial OXPHOS (50 µM for 20 minutes). The fluorescence diminishes when the potential of mitochondrial membrane is altered. First, upon treatment with 6-BrCaQ-C₁₀-TPP, the fluorescence is decreased up to 68% of the initial value (untreated condition) in a time and a dose-dependent effect.. The cell viability at the same time and concentration points was checked by MTT without any cell mortality (Data not shown). TPP-C₁₀-OH (the mitochondrial targeting moiety alone) at the same concentration and time point induced also a decrease up to 35% of the initial value (untreated condition), in a time- and a dose-dependent manner. The magnitude of the decrease is smaller than for the complete molecule. In conclusion, 6-BrCaQ-C₁₀-TPP induces a disruption of the mitochondrial potential compatible with the expected mechanism of action. The results are consistent with both molecules accumulated in mitochondria.

The HSP90 inhibitor without mitochondrial targeting moiety (6-BrCaQ) had a lower impact on the mitochondrial membrane potential, even at higher doses: according to the concentration and the time, it induced either a decrease up to 30% or an increase up to 35% of the potential. As the unconjugated molecule 6-BrCaQ induced an increase in mitochondrial membrane potential, it can be explained by higher ATP levels that can increase mitochondrial membrane potential: this can be caused either by activation of ATP synthase or by inhibition of ATPase³⁷. Yet, HSP90 has an

ATPase activity, which is allosterically decreased by C-terminal inhibitors³⁸. Then, the decrease of potential induced by higher doses can be explained either by induction of apoptosis, or by the inhibition of TRAP1. Indeed, the inhibitor is not specific to one member of the family, at higher concentrations it can inhibit TRAP1 as well, and thus causes the decrease of membrane mitochondrial potential. Such an increase, according to Song, could be caused by mPTP closure³⁹. Papathanassiou showed that F₁-F₀ ATP synthase acted like a co-chaperone of HSP90^{40,41}. It has been shown that HSP90 inhibition induced an increased level of the OSCP subunit of F₀F₁ ATP synthase and a protein accumulation into the mitochondrial matrix.⁴²

In another part of this study, we also envisaged using a fluorescent mitochondria-targeting moiety to localize the drug conjugate by confocal microscopy. Pyridinium vinyltriphenylamines (TP-Py) (Scheme 2A, right) have been described as mitochondrial stainers⁴³. Conjugation of these fluorophores to photosensitizers has already demonstrated that TP-Py can act as cargo for mitochondria⁴⁴. Inspired by this study, 6BrCaQ-C₁₀-TP-2Py (Scheme 2A) was designed as a cargo for visualizing its accumulation inside mitochondria and we applied the synthetic pathway already described for 6BrCaQ-C₁₀-TPP starting with compound **2a** to synthesize the final cargo. We first prepared phenol **7** by Horner-Wadsworth-Emmons reaction on already described dialdehyde **6**. After a nucleophilic substitution of **2a** with derivative **7**, methylation of both pyridines led to the conjugate pyridinium salt 6BrCaQ-C₁₀-TP-2Py in good yield. The photophysical properties ($\lambda_{\text{max}}/\lambda_{\text{em}}$ and ϵ_{max}) of the 6BrCaQ-C₁₀-TP-2Py conjugate were measured and showed to be similar to the reference TP-2Py (Scheme 2B), allowing thus the visualization of the compound by fluorescence microscopy.

Scheme 2. Synthesis of compound **6BrCaQ-C₁₀-TP-2Py** and structure of the parent compound **TP-2Py** and their photophysical properties



Then, the fluorescent 6BrCaQ-C₁₀-TP-2Py was visualized by confocal microscopy in living A549 cells (Figure 4), However no localization in mitochondria was observed. Indeed, colocalization experiments with MitoDeepRed showed no overlap between the two dyes. It seems that 6BrCaQ-C₁₀-TP-2Py is retained in vesicles preventing its accumulation in mitochondria. We can conclude that in this study, TP-2Py did not act as a cargo when is conjugated to a 6BrCaQ inhibitor. This is in accordance with cytotoxicity studies performed on HCT-116; the conjugate is not cytotoxic at 1 μ M (95% viability) whereas 6BrCaQ-C₁₀-TPP is cytotoxic under the same conditions (11% viability at 1 μ M).

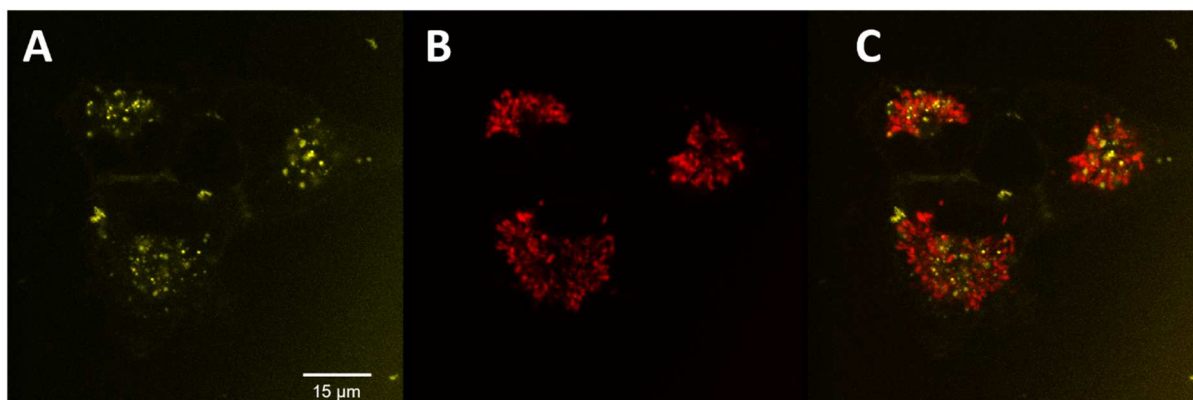


Figure 4. Co-localization experiments with 6BrCaQ-C10-TP-2Py. A549 cells were first incubated with 6BrCaQ-C10-TP-2Py at 2 μ M for 4 h (λ_{exc} 488 nm; λ_{em} = 500-650 nm), then incubated with MitoTracker®DeepRed (100 nM, 45 min, λ_{exc} 633 nm; λ_{em} = 650-800 nm). Confocal images of A) 6BrCaQ-C10-TP-2Py, B) MitoTracker®DeepRed and C) merge.

2.2.4 Targeting of TRAP1 machinery

As the 6BrCaQ is targeting the HSP90 machinery, the addition of C10-TPP moiety is supposed to let the 6BrCaQ-C10-TPP enter the mitochondria and interact with TRAP1. The best way to confirm this interaction is to use Thermal Shift Assay (TSA), Isothermal Titration Calorimetry (ITC) or surface plasmon resonance (SPR) for example. We performed some preliminary experiments with Thermal Shift Assay (see Supporting Information, p16) but we observed an self-assembly of the 6BrCaQ-C10-TPP in aqueous solution not compatible with the study of the interaction (supplementary data). Until now, we are not able to provide an direct proof of the interaction between TRAP1 and 6BrCaQ-C10-TPP. Then we focused our work on providing the indirect proof of the effect of our molecule on TRAP1 activity.

To have a better understanding of the target of 6BrCaQ-C10-TPP, western blots were performed (Figure 5 B→E). First, two well-known partners of TRAP1 were probed, two subunits of succinate dehydrogenase, SDHA and SDHB (Figure 5B and C). They are part of the complex II of mitochondrial respiration and thus their regulation has an important effect on mitochondria metabolism. By using our lead compound, the expression of these two TRAP1 client proteins was found to be decreased in a dose-dependent manner after treatment with 0.1, 0.5, and 1 μ M of 6BrCaQ-C10-TPP for 24 h.

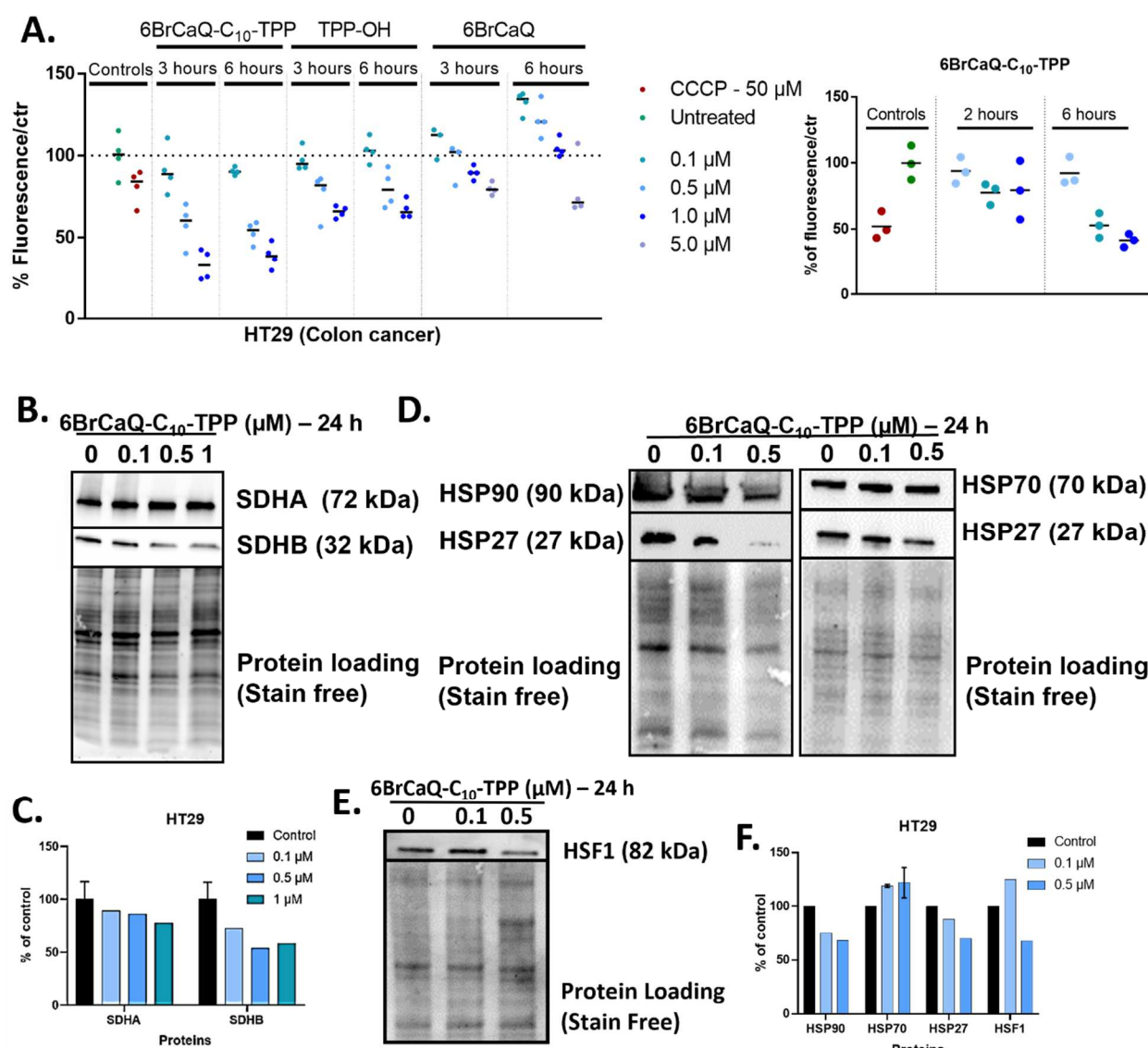


Figure 5. Targeting of mitochondria and TRAP1 machinery. **A.** Decrease of the mitochondrial potential measured by TMRE staining, upon treatment of HT29 cells with 6BrCaQ-C₁₀-TPP for 2 (or 3) and 6 hours. Cells were also treated 20 minutes by 50 μM CCCP as a positive control of the depolarization. This graphs is representative of 3 experiments. **B** and **C.** HT29 cells were treated by 6BrCaQ-C₁₀-TPP for 24 h and then analyzed by western blotting (and densitometry) for TRAP1 protein partners, SDHA and B. **D** and **E.** HT29 cells are treated by 6BrCaQ-C₁₀-TPP for 24 h and then analyzed by western blotting for Heat shock proteins (HSP90, HSP70, HSP27) and HSF-1. **F.** Densitometry analysis of D and E panels. All the western blots were duplicated.

It's well known that TRAP1 controls SDH activity^{45–47}. However, Chae et al., have shown that SDH-B was degraded by TRAP inhibition by Gamitrinib or TRAP1 silencing⁴⁸. Indeed, even if TRAP1 inhibits SDH, it also stabilizes the subunit B. They also showed that Gamitrinib and silencing of TRAP1 induced a decrease in the activity of the succinate dehydrogenase, probably due to its degradation. This is consistent with the decrease of SDH-A/B levels showed by western blot (Figure 5B, C).

The expression of several heat-shock proteins involved in the stress response and in the HSP90 machinery were evaluated as well: HSP27, HSP70 and HSP90 (Figure 5D and E). **In addition, the expression of the transcription factor HSF1 was also checked in order to check the potential induction of the Heat Shock Response as it is observed for**

HSP90 N-terminal inhibitors that induce a Heat-shock-response by releasing a transcription factor (HSF1) of the genes of HSP27, HSP70 and HSP90. This increase in transcription leads to opposition to apoptosis and, thus, to resistance to treatment⁷. McAlpine and Wang showed that C-terminal inhibitors don't have the same phenotype as N-terminal ones and do not induce heat-shock response¹². In our work, this is important to check that the levels of these genes are not increasing. Then, we showed by western blot that 6BrCaQ-C10-TPP stabilizes or decreases the levels of HSP27 and HSP70 without triggering the HSR. In fact, HSF1 is not induced but is degraded for 0.5 μ M of treatment as shown in the Figure 5D. This result was already observed with 6BrCaQ in PC-3 cell lines as we reported previously: liposomal 6-BrCaQ stabilized levels of HSP70 and decreased level of HSP90¹⁶. However, in MDA cell line, it decreased HSP90 and HSP70 proteins levels, nonetheless gene expression of HSP70 and HSP90 were stable, whereas HSP27 gene expression levels were reduced¹³. Their transcription factor, HSF1, was also analyzed, and showed a slight decrease upon treatment. TRAP1 expression was not modified by the treatment (data not shown). These results confirm that 6BrCaQ-C10-TPP induces inhibition of TRAP1 without inducing the heat-shock response. This is consistent also with Gaminitrib results: even if the N-terminal inhibitor 17-AAG induced an increase in HSP70 protein level, some of the Gamitribins, included the one linked to a TPP⁺ moiety, stabilized or decreased HSP70 levels⁴⁹. The specific TRAP1 inhibitor without mitochondrial vehicle DN401 also induced a decrease in HSP70 protein levels¹⁸.

3. Conclusions

In summary, we designed and synthesized a series of substituted 6BrCaQ-TPP conjugates **3a-f** and **5** bearing variable linker lengths in the aim to target selectively the TRAP1 machinery. From this SAR study, 6BrCaQ-C10-TPP (**3a**) was found to be the strongest analogue displaying the anti-proliferative activity with mean GI₅₀ values at a nanomolar level in a diverse set of human cancer cells (GI₅₀ = 0.008-0.30 μ M) including MDA-MB-231, HT-29, HCT116, K562 and PC-3 cancer cell lines. This study showed that the lead compound 6BrCaQ-C10-TPP exhibited radically different properties profile from the parent compound 6BrCaQ by inducing a significant mitochondrial membrane disruption. In addition, 6BrCaQ-C10-TPP is able to interfere with TRAP1 function and to inhibit proliferation of colon carcinoma cells without inducing the heat-shock response HSF1.

4. Experimental

4.1. Chemistry.

4.1.a. General considerations

The compounds were all identified by usual physical methods, i.e. ¹H-NMR, ¹³C-NMR, IR, MS. ¹H and ¹³C NMR spectra were measured in CDCl₃ with a Bruker Avance 300 or Bruker Avance 400. ¹H chemical shifts are reported in ppm from an internal standard TMS or of residual chloroform (7.27 ppm). The following abbreviations are used: m (multiplet), s (singlet), d (doublet), br s (broad singlet), t (triplet), dd (doublet of doublet), td (triplet of doublet). ¹³C chemical shifts are reported in ppm from the central peak of CDCl₃ (77.14). IR spectra were measured on a Bruker Vector 22 spectrophotometer (neat, cm⁻¹). Elemental analyses were performed with a Perkin-Elmer 240 analyzer. Mass spectra were obtained with a LCT Micromass spectrometer. Analytical TLC was performed on Merck precoated silica gel 60F plates. Merck silica gel 60 (230-400 mesh) was used for column chromatography. Visualization was achieved with UV light and phosphomolybdic acid reagent unless otherwise stated. Monosodium novobiocin salt was purchased from Sigma-Aldrich; all other reagents were of high grade and were used without further purification.

4.1.b. Procedure for the synthesis of N-(6-bromo-1-methyl-2-oxo-1,2-dihydroquinolin-3-yl)-4-hydroxybenzamide **1a**

A flame-dried resealable tube was charged with Pd(OAc)₂ (10 mol%, 14.7 mg), Xantphos (20 mol%, 76 mg), dibromoquinolinone (0.66 mmol, 210 mg), 4-hydroxybenzamide (1.01 equiv, 0.66 mmol, 92 mg) and Cs₂CO₃ (2 equiv, 1.32 mmol, 428 mg). The tube was capped with a rubber septum, evacuated and backfilled with argon; this evacuation/ backfill sequence was repeated one additional time. The 1,4-dioxane (13 mL) was added through the septum. The Schlenk tube was sealed, and the mixture was stirred at 130 °C for 1 h 30. At the end of the reaction, the color of the mixture changed from bright yellow to orange. The resulting suspension was cooled to room temperature and filtered through a pad of Celite eluting with DCM/MeOH (8:2), and the inorganic salts were removed. The product was obtained as a beige powder.

Yield: 91%; m.p.: 222-224 °C; TLC: R_f = 0.43 (Cyclohexane/EtOAc: 5/5); IR (neat): 3401, 3300, 3214, 3100, 2401, 2312, 2199, 2176, 2095, 1672, 1542, 1449, 1215, 1211, 1033 cm⁻¹; ¹H NMR (300 MHz, DMSO) δ 10.30 (s, 1H), 9.37 (s, 1H), 8.69 (s, 1H), 8.04 (d, J = 2.0 Hz, 1H), 7.82 (d, J = 8.6 Hz, 2H), 7.68 (dd, J = 8.9, 2.0 Hz, 1H), 7.53 (d, J = 9.0 Hz, 1H), 6.92 (d, J = 8.6 Hz, 2H), 3.75 (s, 3H); ¹³C NMR (75 MHz, DMSO) δ 164.6 (C), 161.4 (C), 157.2 (C), 134.5 (C), 130.9 (CH), 129.9 (CH), 129.3 (2CH), 128.5 (C), 124.0 (C), 122.3 (C), 118.4 (CH), 117.0 (CH), 115.6 (2CH), 115.0 (C), 30.4 (Me). HR-MS (ESI positive, m/z): found 373.0191 ([M+H]⁺), calcd. for C₁₇H₁₄N₂O₃Br (M+H): 373.0182.

4.1.c. Procedure for the synthesis of *N*-(6-bromo-1-methyl-2-oxo-1,2-dihydroquinolin-3-yl)-4-((10-bromodecyl)oxy)benzamide **2a**

To a solution of 6BrCaOH **1a** (140 mg, 0.38 mmol) in anhydrous acetone (12.5 mL), K₂CO₃ (415 mg, 3 mmol, 8 equiv) and 1,10-dibromodecane (8 equiv, 3 mmol, 900 mg) were added. The mixture was stirred under reflux (60 °C) overnight. Then K₂CO₃ was removed by filtration, and the solvent was evaporated under vacuum. The crude products were purified by flash chromatography on silica gel using eluent 10 to 30 % EtOAc/ Cyclohexane.

The product **2a** was obtained as white powder, yield 76% (205 mg); m.p.: 111-112 °C; TLC: R_f = 0.36 (Cyclohexane/EtOAc: 7/3); IR (neat): 1766, 1675, 1604, 1504, 1471, 1243, 1175, 1053 cm⁻¹; ¹H NMR (300 MHz, CDCl₃) δ 9.31 (s, 1H), 8.78 (s, 1H), 7.90 (d, J = 8.7 Hz, 2H), 7.75 (d, J = 2.0 Hz, 1H), 7.55 (dd, J = 8.9, 2 Hz, 1H), 7.23 (d, J = 8.9 Hz, 1H), 6.97 (d, J = 8.7 Hz, 2H), 4.02 (t, J = 6.5 Hz, 2H), 3.81 (s, 3H), 3.41 (t, J = 6.8 Hz, 2H), 1.94 – 1.70 (m, 4H), 1.48 – 1.20 (m, 12H); ¹³C NMR (75 MHz, CDCl₃) δ 165.6 (C), 162.6 (C), 158.1 (C), 134.5 (C), 131.3 (CH), 130.7 (CH), 129.3 (2CH), 129.0 (C), 126.1 (C), 123.1 (C), 118.7 (CH), 116.2 (C), 115.7 (CH), 114.7 (2CH), 68.4 (CH₂), 34.2 (CH₂), 32.9 (CH₂), 30.6 (CH₃), 29.6 (CH₂), 29.5 (CH₂), 29.4 (CH₂), 29.2 (CH₂), 28.9 (CH₂), 28.3 (CH₂), 26.1 (CH₂). HR-MS (ESI positive, m/z): found 373.0191 ([M+H]⁺), calcd. for C₁₇H₁₄N₂O₃Br (M+H): 373.0182.

4.1.d. Procedure for the synthesis of (10-(4-((6-bromo-1-methyl-2-oxo-1,2-dihydroquinolin-3-yl)carbamoyl)phenoxy)decyl)triphenylphosphonium **3a**

A mixture of brominated product **2a** (70 mg, 0.27 mmol) and PPh₃ (350 mg, 1.33 mmol, 5 equiv) in 5 ml anhydrous acetonitrile was stirred at 100 °C for two days. Evaporation of the solvent. The crude product were purified by flash chromatography with eluent MeOH/DCM 0 to 5% to afford the product **3a** as white powder, yield: 50% (0.13 mmol, 110 mg); m.p.: 127-129 °C; TLC: R_f = 0.29 (EtOAc/MeOH: 8/2); IR (neat): 1639, 1605, 1527, 1504, 1486, 1260, 1176, 909 cm⁻¹; ¹H NMR (300 MHz, MeOD) δ 8.57 (s, 1H), 7.95 – 7.86 (m, 4H), 7.85 – 7.71 (m, 13H), 7.68 (d, J = 2.1 Hz, 1H), 7.56 (dd, J = 9.1, 2.1 Hz, 1H), 7.39 (d, J = 9.1 Hz, 1H), 6.97 (d, J = 8.8 Hz, 2H), 4.01 (t, J = 6.4 Hz, 2H), 3.76 (s, 3H), 3.41 (ddd, J = 13.6, 9.1, 6.8 Hz, 2H), 1.84 – 1.73 (m, 2H), 1.72 – 1.62 (m, 2H), 1.61 – 1.52 (m, 2H), 1.51 – 1.43 (m, 2H), 1.41 – 1.22 (m, 8H); ¹³C NMR (50 MHz, MeOH) δ 166.4 (C), 163.8 (C), 158.7 (C), 136.2 (3CH), 136.2 (C),

135.6 (CH), 134.9 (3CH), 134.7 (3CH), 132.3 (3CH), 131.6 (3CH), 131.4 (CH), 131.1 (2CH), 130.1 (3CH), 129.6 (C), 126.5 (C), 123.7 (C), 120.8 (C), 119.7 (CH), 119.1 (C), 117.5 (CH), 116.9 (C), 115.5 (2CH), 69.3 (CH₂), 31.7 (CH₂), 31.4 (CH₂), 31.1 (CH₂), 30.4 (CH₃), 30.3 (CH₂), 29.9 (CH₂), 27.0 (CH₂), 23.6 (CH₂), 23.2 (CH₂), 22.2 (CH₂); ³¹P NMR (81 MHz, MeOH) δ 74.49. HR-MS (ESI positive, m/z): found 773.2512 ([M+Na]⁺), calcd. for C₄₀H₅₀N₂O₅BrPNa (M+Na): 773.2581.

4.1.e. Procedure for the synthesis of (3-(4-((6-bromo-1-methyl-2-oxo-1,2-dihydroquinolin-3-yl)carbamoyl)phenoxy)propyl)triphenylphosphonium **3b**

A flame-dried resealable tube was charged with 6BrCaQ-OH **1a** (37 mg), (3-bromopropyl)triphenylphosphonium (1.2 equiv, 46 mg), K₂CO₃ (8 equiv, 108 mg). The tube was capped with a rubber septum, evacuated and backfilled with argon; this evacuation/ backfill sequence was repeated one additional time. The DMF (3.7 mL) was added through the septum. The Schlenk tube was sealed, and the mixture was stirred at 60 °C for 2h. The solvent was evaporated under vacuum (toluene azeotrope evaporation can be used to help remove traces of DMF). A purification by flash chromatography was conducted to obtain the desired product (DCM / MeOH). Due to the carbon-phosphorus coupling in ¹³C-NMR more peaks are observed in ¹³C-NMR.

The product **3b** was obtained as a whitish solid. Yield : 56%; TLC : R_f IF ¹H NMR (300 MHz, MeOD) δ 8.73 (s, 1H), 8.46 (s, 1H), 7.99 – 7.73 (m, 18H), 7.66 (dd, J = 9.0, 1.8 Hz, 1H), 7.50 (d, J = 9.1 Hz, 1H), 7.09 (d, J = 8.7 Hz, 2H), 4.26 (t, J = 5.4 Hz, 2H), 3.84 (s, 3H), 3.71 – 3.58 (m, 2H), 2.31 – 2.14 (m, J = 22.1 Hz, 2H). ¹³C NMR (75 MHz, MeOD) δ = 167.12 (C), 163.2 (C), 159.3 (C), 136.4 (3CH), 136.4 (3CH), 136.1 (C), 134.9 (6CH), 134.8 (6CH), 132.7 (CH), 131.7 (6CH), 131.5 (6CH), 130.4 (2CH), 129.9 (C), 127.8 (C), 124.0 (C), 120.7 (CH), 120.3 (C), 119.1 (C), 117.6 (CH), 117.1 (C), 115.8 (2CH), 68.2 (CH₂), 31.0 (CH₃), 29.6 (CH₂), 23.7 (CH₂), 19.7 (CH₂). HR-MS (ESI positive, m/z): found 675.1417 ([M]⁺), calcd. for C₃₈H₃₃N₂O₃PBr (M⁺): 675.1412.

4.1.f. Procedure for the synthesis of (5-(4-((6-bromo-1-methyl-2-oxo-1,2-dihydroquinolin-3-yl)carbamoyl)phenoxy)pentyl)triphenylphosphonium **3c**

A flame-dried resealable tube was charged with 6BrCaQ-OH **1a** (37 mg), (4-bromobutyl)triphenylphosphonium (1.2 equiv, 48 mg), K₂CO₃ (8 equiv, 108 mg). The tube was capped with a rubber septum, evacuated and backfilled with argon; this evacuation/ backfill sequence was repeated one additional time. The DMF (3.7 mL) was added through the septum. The Schlenk tube was sealed, and the mixture was stirred at 60 °C for 2h. The solvent was evaporated under vacuum (toluene azeotrope evaporation can be used to help remove traces of DMF). A purification by flash chromatography was conducted to obtain the desired product (DCM / MeOH). Due to the carbon-phosphorus coupling in ¹³C-NMR more peaks are observed in ¹³C-NMR.

The product **3c** was obtained as a whitish solid. Yield : 46%; ¹H NMR (300 MHz, MeOD) δ 8.64 (s, 1H), 7.96 – 7.73 (m, 19H), 7.60 (dd, J = 9.0, 1.7 Hz, 1H), 7.44 (d, J = 9.0 Hz, 1H), 6.99 (d, J = 8.7 Hz, 2H), 4.15 (t, J = 5.8 Hz, 2H), 3.79 (s, 3H), 3.60 – 3.49 (m, 2H), 2.10 (dd, J = 12.9, 6.6 Hz, 2H), 1.97 – 1.87 (m, 2H). ¹³C NMR (75 MHz, MeOD) δ = 167.0 (C), 163.6 (C), 159.1 (C), 136.3 (3CH), 136.0 (C), 134.9 (6CH), 134.8 (6CH), 132.6 (CH), 131.7 (6CH), 131.5 (6CH), 131.4 (CH), 130.3 (2HC), 129.8 (C), 127.3 (C), 123.9 (C), 120.4 (C), 119.3 (C), 117.6 (CH), 117.1 (C), 115.7 (2CH), 67.8 (CH₂), 31.0 (CH₂), 30.8 (CH₂), 30.6 (CH₃), 22.7 (CH₂), 22.0 (CH₂), 20.3 (CH₂), 20.3 (CH₂). HR-MS (ESI positive, m/z): found 689.1569 ([M]⁺), calcd. for C₃₉H₃₅N₂O₃PBr (M⁺): 689.1569.

4.1.g. Procedure for the synthesis of (5-(4-((6-bromo-1-methyl-2-oxo-1,2-dihydroquinolin-3-yl)carbamoyl)phenoxy)pentyl)triphenylphosphonium **3d**

A flame-dried resealable tube was charged with 6BrCaQ-OH (34 mg), (5-bromopentyl)triphenylphosphonium (1.2 equiv, 53.2 mg), K₂CO₃ (8 equiv, 100 mg). The tube was capped with a rubber septum, evacuated and backfilled with argon; this evacuation/ backfill sequence was repeated one additional time. The DMF (3.4 mL) was added through the septum. The Schlenk tube was sealed, and the mixture was stirred at 60 °C for 2h. The solvent was evaporated under vacuum (toluene azeotrope evaporation can be used to help remove traces of DMF). A purification by flash chromatography was conducted to obtain the desired product (DCM / MeOH). Due to the carbon-phosphorus coupling in ¹³C-NMR more peaks are observed in ¹³C-NMR.

The product **3d** was obtained as a whitish solid. Yield : 55%; The structure was confirmed by ¹H NMR. ¹³C NMR (75 MHz, MeOD) δ = 167.0 (C), 163.8 (C), 159.1 (C), 136.3 (3CH), 136.3 (3CH), 136.0 (C), 134.9 (6CH), 134.8 (6CH), 132.6 (CH), 131.6 (6CH), 131.5 (6CH), 130.3 (2CH), 129.8 (C), 127.1 (C), 123.9 (C), 120.5 (C), 120.4 (CH), 119.4 (C), 117.6 (CH), 117.1 (C), 115.6 (2CH), 69.0 (CH₂), 33.0 (CH₂), 31.0 (CH₃), 29.3 (CH₂), 28.5 (CH₂), 28.3 (CH₂), 23.7 (CH₂), 23.4 (CH₂), 23.3 (CH₂), 23.1 (CH₂), 22.4 (CH₂). HR-MS (ESI positive, m/z): found 703.1725 ([M]⁺), calcd. for C₄₀H₃₇N₂O₃PBr (M⁺): 703.1725.

4.1.h. Procedure for the synthesis of (7-(4-((6-bromo-1-methyl-2-oxo-1,2-dihydroquinolin-3-yl)carbamoyl)phenoxy)heptyl)triphenylphosphonium **3e**

A flame-dried resealable tube was charged with 6BrCaQ-OH **1a** (37 mg), (7-bromoheptyl)triphenylphosphonium (1.2 equiv, 53 mg), K₂CO₃ (8 equiv, 108 mg). The tube was capped with a rubber septum, evacuated and backfilled with argon; this evacuation/ backfill sequence was repeated one additional time. The DMF (3.7 mL) was added through the septum. The Schlenk tube was sealed, and the mixture was stirred at 60 °C for 2h. The solvent was evaporated under vacuum (toluene azeotrope evaporation can be used to help remove traces of DMF). A purification by flash chromatography was conducted to obtain the desired product (DCM / MeOH). Due to the carbon-phosphorus coupling in ¹³C-NMR more peaks are observed in ¹³C-NMR.

The product **3e** was obtained as a whitish solid. Yield : 45%; ¹H NMR (300 MHz, MeOD) δ 8.64 (s, 1H), 7.92 – 7.75 (m, 19H), 7.60 (dd, *J* = 9.0, 2.2 Hz, 1H), 7.44 (d, *J* = 9.1 Hz, 1H), 6.98 (d, *J* = 8.9 Hz, 2H), 4.03 (t, *J* = 6.3 Hz, 2H), 3.81 (s, 3H), 3.46 – 3.38 (m, 2H), 1.81 – 1.57 (m, 6H), 1.46 (d, *J* = 3.0 Hz, 4H). ¹³C NMR (75 MHz, MeOD) δ = 167.0 (C), 164.0 (C), 159.1 (C), 136.3 (3CH), 136.0 (C), 134.9 (6CH), 134.7 (6CH), 132.6 (CH), 131.6 (6CH), 131.5 (6CH), 130.3 (2CH), 129.8 (C), 126.9 (C), 123.9 (C), 120.6 (C), 120.3 (CH), 119.4 (C), 117.6 (CH), 117.1 (C), 115.6 (2CH), 69.2 (CH₂), 33.5 (CH₂), 31.6 (CH₂), 31.4 (CH₂), 31.0 (CH₂), 30.0 (CH₂), 29.5 (CH₃), 27.5 (CH₂), 26.7 (CH₂), 23.5 (CH₂), 23.4 (CH₂), 23.0 (CH₂), 22.4 (CH₂). HR-MS (ESI positive, m/z): found 731.2040 ([M]⁺), calcd. for C₄₂H₄₁N₂O₃PBr (M+H): 731.2038.

4.1.i. Procedure for the synthesis of (10-(4-((6-bromo-1-methyl-2-oxo-1,2-dihydroquinolin-3-yl)carbamoyl)phenoxy)decyl)triphenylphosphonium **3a**

A flame-dried resealable tube was charged with 6BrCaQ-OH **1a** (300 mg), (10-bromodecyl)triphenylphosphonium (2 equiv, 540 mg), K₂CO₃ (4 equiv, 420 mg). The tube was capped with a rubber septum, evacuated and backfilled with argon; this evacuation/ backfill sequence was repeated one additional time. The DMF (15 mL) was added through the

1 septum. The Schlenk tube was sealed, and the mixture was stirred at 60 °C for 2h. The solvent was evaporated under
2 vacuum (toluene azeotrope evaporation can be used to help remove traces of DMF). A purification by flash
3 chromatography was conducted to obtain the desired product (DCM / MeOH). An impurity with a very similar polarity
4 as the desired product **3a** was separated using preparative HP-LC and obtained as a whitish solid. Yield : 24%: The
5 structure was confirmed by ¹H NMR and HR-MS.

6 *4.1.j. Procedure for the synthesis of (10-(4-((1-methyl-2-oxo-1,2-dihydroquinolin-3-yl)carbamoyl)phenoxy)decyl)triphenylphosphonium 5*

8 A flame-dried resealable tube was charged with CaQ-OH **1b** (30 mg), (10-bromodecyl)triphenylphosphonium (2 equiv,
9 54 mg), K₂CO₃ (4 equiv, 42 mg). The tube was capped with a rubber septum, evacuated and backfilled with argon; this
10 evacuation/ backfill sequence was repeated one additional time. The DMF (1.5 mL) was added through the septum. The
11 Schlenk tube was sealed, and the mixture was stirred at 60 °C for 2h. The solvent was evaporated under vacuum
12 (toluene azeotrope evaporation can be used to help remove traces of DMF). Due to the carbon-phosphorus coupling in
13 ¹³C-NMR more peaks are observed in ¹³C-NMR.

14 The product **5** was obtained as a whitish solid. ¹H NMR (300 MHz, MeOD) δ 8.79 (s, 1H), 8.24 (s, 1H), 8.07 – 7.70 (m,
15 17H), 7.67 (d, *J* = 7.8 Hz, 1H), 7.58 (d, *J* = 3.6 Hz, 2H), 7.38 – 7.30 (m, 1H), 7.05 (d, *J* = 8.9 Hz, 2H), 4.07 (t, *J* = 6.3
16 Hz, 2H), 3.85 (s, 3H), 3.46 – 3.37 (m, *J* = 12.7, 10.2 Hz, 2H), 1.88 – 1.74 (m, *J* = 14.3, 6.5 Hz, 2H), 1.73 – 1.62 (m, *J* =
17 7.6 Hz, 2H), 1.61 – 1.44 (m, *J* = 13.3, 5.8 Hz, 4H), 1.42 – 1.26 (m, 8H). ¹³C NMR (75 MHz, MeOD) δ = 165.9 (C),
18 162.7 (C), 158.1 (C), 135.7 (C), 134.9 (3CH), 134.8 (3CH), 133.4 (6CH), 133.3 (6CH), 130.2 (6CH), 130.0 (6CH),
19 128.8 (3CH), 128.2 (CH), 127.4 (C), 125.7 (C), 123.1 (C), 120.9 (CH), 120.8 (CH), 119.2 (C), 118.0 (C), 114.3 (2CH),
20 114.2 (CH), 67.9 (CH₂), 30.3 (CH₂), 30.0 (CH₂), 29.5 (CH₃), 29.3 (CH₂), 29.0 (CH₂), 28.8 (CH₂), 28.8 (CH₂), 28.7
21 (CH₂), 28.4 (CH₂), 25.6 (CH₂), 22.1 (CH₂), 22.1 (CH₂), 22.0 (CH₂), 22.0 (CH₂), 20.9 (CH₂). HR-MS (ESI positive,
22 *m/z*): found 695.3399 ([M]⁺), calcd. for C₄₅H₄₈N₂O₃P (M⁺): 695.3403.

23 *4.1.k. Procedure for the synthesis of (12-(4-((6-bromo-1-methyl-2-oxo-1,2-dihydroquinolin-3-yl)carbamoyl)phenoxy)decyl)triphenylphosphonium 3f*

25 A flame-dried resealable tube was charged with 6BrCaQ-OH (60 mg), (12-bromododecyl)triphenylphosphonium (1.8
26 equiv, 180 mg), K₂CO₃ (4 equiv, 88.5 mg). The tube was capped with a rubber septum, evacuated and backfilled with
27 argon; this evacuation/ backfill sequence was repeated one additional time. The DMF (3 mL) was added through the
28 septum. The Schlenk tube was sealed, and the mixture was stirred at 60 °C for 2h. The solvent was evaporated under
29 vacuum (toluene azeotrope evaporation can be used to help remove traces of DMF). A purification by flash
30 chromatography (DCM / MeOH) furnished the desired product in 46% yield as a whitish solid. ¹H NMR (300 MHz,
31 MeOD) δ 8.6 (s, 1H), 8.34 (s, 1H), 7.93 – 7.66 (m, 18H), 7.59 (dd, *J* = 8.9 Hz, 1H), 7.42 (d, *J* = 9.0 Hz, 1H), 7.00 (d, *J*
32 = 8.7 Hz, 2H), 4.04 (t, *J* = 6.4 Hz, 2H), 3.78 (s, 3H), 3.44 – 3.35 (m, 2H), 1.88 – 1.74 (m, 2H), 1.73 – 1.61 (m, *J* = 7.4
33 Hz, 2H), 1.57 – 1.44 (m, 4H), 1.42 – 1.21 (m, 12H). ¹³C NMR (75 MHz, MeOD) δ = 165.1 (C), 162.5 (C), 157.4 (C),
34 134.9 (3CH), 134.8 (3CH), 134.3 (C), 133.4 (6CH), 133.3 (6CH), 130.9 (CH), 130.2 (6CH), 130.0 (6CH), 129.8 (CH),
35 128.8 (2CH), 128.23 (C), 125.21 (C), 122.35 (C), 119.13 (C), 118.40 (CH), 117.98 (C), 116.03 (CH), 115.56 (C),
36 114.11 (2CH), 67.9 (CH₂), 30.3 (CH₂), 30.1 (CH₂), 29.6 (CH₃), 29.2 (CH₂), 29.1 (CH₂), 29.0 (CH₂), 28.8 (CH₂), 28.5
37 (CH₂), 25.6 (CH₂), 22.2 (CH₂), 22.1 (CH₂), 21.6 (CH₂), 20.9 (CH₂).

38 *4.1.l. Procedure for the synthesis of (12-(4-((6-bromo-1-methyl-2-oxo-1,2-dihydroquinolin-3-yl)carbamoyl)phenoxy)dodecyl)triphenylphosphonium 7*

A flame-dried resealable tube was charged with 6BrCaQ-OH **1a** (60 mg), (12-bromododecyl)triphenylphosphonium (1.8 equiv, 180 mg), K₂CO₃ (4 equiv, 88.5 mg). The tube was capped with a rubber septum, evacuated and backfilled with argon; this evacuation/ backfill sequence was repeated one additional time. The DMF (3 mL) was added through the septum. The Schlenk tube was sealed, and the mixture was stirred at 60 °C for 2 h. The solvent was evaporated under vacuum (toluene azeotrope evaporation can be used to help remove traces of DMF). A purification by flash chromatography was conducted to obtain the desired product (DCM / MeOH). Due to the carbon-phosphorus coupling in ¹³C-NMR more peaks are observed in ¹³C-NMR. The product **3f** was obtained as a whitish solid. Completion of the reaction observed by TLC. NMR (300 MHz, MeOD) δ 8.61 (s, 1H), 8.34 (s, 1H), 7.93 – 7.66 (m, 18H), 7.59 (dd, *J* = 8.9 Hz, 1H), 7.42 (d, *J* = 9.0 Hz, 1H), 7.00 (d, *J* = 8.7 Hz, 2H), 4.04 (t, *J* = 6.4 Hz, 2H), 3.78 (s, 3H), 3.44 – 3.35 (m, 2H), 1.88 – 1.74 (m, 2H), 1.73 – 1.61 (m, *J* = 7.4 Hz, 2H), 1.57 – 1.44 (m, 4H), 1.42 – 1.21 (m, 12H). ¹³C NMR (75 MHz, MeOD) δ = 165.1 (C), 162.5 (C), 157.4 (C), 134.9 (3CH), 134.9 (3CH), 134.3 (C), 133.4 (6CH), 133.3 (6CH), 131.0 (CH), 130.2 (6CH), 130.0 (6CH), 129.8 (CH), 128.8 (2CH), 128.2 (C), 125.2 (C), 122.4 (C), 119.1 (C), 118.4 (CH), 118.0 (C), 116.0 (CH), 115.6 (C), 114.1 (2CH), 68.0 (CH₂), 30.4 (CH₂), 30.1 (CH₂), 29.7 (CH₃), 29.2 (CH₂), 29.1 (CH₂), 29.0 (CH₂), 28.8 (CH₂), 28.5 (CH₂), 25.7 (CH₂), 22.2 (CH₂), 22.1 (CH₂), 21.6 (CH₂), 21.0 (CH₂). R-MS (ESI positive, *m/z*): found 801.2820 ([M]⁺), calcd. for C₄₇H₅₁N₂O₃PBr (M⁺): 801.2820.

4.1.m. Procedure for the synthesis of 4-(bis(4-((*E*)-2-(pyridin-4-yl)vinyl)phenyl)amino)phenol **7**

In dry THF, diethyl [(pyridin-4-yl)methyl]phosphonate (2.2 eq., 0.69 mmol, 158.9 mg, 0.14 mL) and NaH (4 eq., 60% in mineral oil, 1.26 mmol, 50.4 mg) were mixed. After 15 minutes stirring, aldehyde **6** (1 eq., 0.32 mmol, 100 mg) was added to the solution and the resulting mixture was stirred at room temperature overnight. Water (50 mL) was added to the residue and the aqueous phase obtained was extracted twice with DCM. The organic phase was washed twice with brine, dried over MgSO₄ and evaporated. The crude products were purified by flash chromatography on silica gel using eluent 100 to 90 % DCM/ EtOH.

The product **7** was obtained as a white powder, yield 76% (205 mg). m.p. >220°C. TLC: R_f = 0.46 (DCM/EtOH: 95/5) ¹H NMR (300 MHz, DMSO) δ 9.55 (s, 1H), 8.51 (d, *J* = 6.0 Hz, 4H), 7.62 – 7.37 (m, 10H), 7.08 (d, *J* = 16.5 Hz, 2H), 7.01 – 6.96 (m, 6H), 6.81 (d, *J* = 9.0 Hz, 2H). ¹³C NMR (75 MHz, DMSO) δ 155.2 (C), 150.0 (CH), 147.6 (C), 144.6 (C), 137.3 (C), 132.6 (CH), 129.7 (C), 128.4 (CH), 128.3 (CH), 123.8 (CH), 121.9 (CH), 120.6 (CH), 116.6 (CH). MS (ESI⁺): *m/z* 468.4 [M+H]

4.1.n. Procedure for the synthesis of 4-((10-(4-(bis(4-((*E*)-2-(pyridin-4-yl)vinyl)phenyl)amino)phenoxy)decyl)oxy)-*N*-(6-bromo-1-methyl-2-oxo-1,2-dihydroquinolin-3-yl)benzamide **8**

To a solution of compound **7** (1 equiv, 0.05 mmol, 24 mg) in anhydrous DMF (12.5 mL) was added Cs₂CO₃ (5 equiv, 0.25 mmol, 82 mg). After stirring 15 min, brominated product **2a** (1 equiv, 0.05 mmol, 30 mg) was added and the mixture was stirred overnight at room temperature. The reaction mixture was then concentrated under reduced pressure. 10 mL of water were added to the residue and the aqueous phase obtained was extracted twice with DCM. The organic phase was washed twice with brine, dried over MgSO₄ and evaporated. The crude products were purified by flash chromatography on silica gel using eluent 20 to 60 % EtOAc/ Cyclohexane.

The product **8** was obtained as a red powder, yield 82% (41 mg). m.p.: 111-112 °C. TLC: R_f = 0.64 (DCM/EtOH: 95/5) ¹H NMR (300 MHz, CDCl₃) δ 9.30 (s, 1H), 8.77 (s, 1H), 8.54 (s, 4H), 7.90 (d, *J* = 8.5 Hz, 2H), 7.74 (d, *J* = 2.0 Hz, 1H), 7.55 (dd, *J* = 9.0, 2.0 Hz, 1H), 7.39 (d, *J* = 8.5 Hz, 4H), 7.33 (d, *J* = 4.0 Hz, 4H), 7.23 – 7.21 (m, 3H), 7.10 – 7.04 (m, 8H), 6.97 (d, *J* = 8.5 Hz, 2H), 6.90 (d, *J* = 3.0 Hz, 2H), 6.85 (d, *J* = 4.0 Hz, 2H), 4.02 (t, *J* = 6.5 Hz, 2H), 3.96 (t, *J* = 6.5

Hz, 2H), 3.79 (s, 3H), 1.84 – 1.78 (m, 4H), 1.56 – 1.31 (m, 12H). ¹³C NMR (75 MHz, CDCl₃) δ 165.5 (C), 162.6 (C), 158.1 (C), 156.7 (C), 150.2 (CH), 148.2 (C), 145.1 (C), 139.5 (C), 134.5 (C), 132.8 (CH), 131.3 (CH), 130.7 (CH), 130.1 (C), 129.3 (CH), 129.0 (C), 128.1 (CH), 128.0 (CH), 126.1 (C), 124.1 (CH), 123.1 (C), 122.8 (CH), 120.8 (CH), 118.7 (CH), 116.2 (C), 115.7 (CH), 114.7 (CH), 68.4 (CH₂), 30.6 (CH₃), 29.8 (CH₂), 29.6 (CH₂), 29.5 (CH₂), 29.2 (CH₂), 26.2 (CH₂), 26.1 (CH₂). MS (ESI+): m/z 980.9 [M+H]

4.1.o. Procedure for the synthesis of 4,4'-((1E,1'E)-(((4-((10-(4-((6-bromo-1-methyl-2-oxo-1,2-dihydroquinolin-3-yl)carbamoyl)phenoxy)decyl)oxy)phenyl)azanediyl)bis(4,1-phenylene))bis(ethene-2,1-diyl))bis(1-methylpyridin-1-ium) 6BrCaQ-C10-TP-2Py

A large excess of methyl iodide (1 mL) was added to a solution of compound **8** (38 mg, 0.04mmol) in MeOH/DCM (1/1-4mL). The solution was stirred at 40°C overnight. The desired compound was then precipitated in Et₂O to afford compound **6BrCaQ-C10-TP2Py** as a red solid (28 mg, 57 %). m.p.: 189-189 °C. ¹H NMR (300 MHz, DMSO) δ 9.39 (s, 1H), 8.80 (d, *J* = 6.5 Hz, 4H), 8.66 (s, 1H), 8.15 (d, *J* = 6.5 Hz, 4H), 7.99 (d, *J* = 5.0 Hz, 2H), 7.95 – 7.82 (m, 3H), 7.66 (d, *J* = 8.5 Hz, 5H), 7.51 (d, *J* = 9.0 Hz, 1H), 7.34 (d, *J* = 16.0 Hz, 2H), 7.19 – 6.94 (m, 10H), 4.23 (s, 6H), 4.05 (t, *J* = 6.0 Hz, 2H), 3.97 (t, *J* = 6.0 Hz, 2H), 3.73 (s, 3H), 1.82 - 1.66 (m, 5H), 1.51 - 1.27 (m, 12H). ¹³C NMR (75 MHz, DMSO) δ 164.4 (C), 161.9 (C), 157.1 (C), 156.7 (C), 152.7 (Cq), 148.5 (Cq), 144.8 (CH), 140.2 (CH), 138.0(C), 134.5 (C), 131.0 (CH), 129.9 (CH), 129.6 (CH), 129.1 (CH), 129.1 (C), 128.4 (CH), 128.4 (C), 125.4 (C), 123.0 (CH), 122.2 (Cq), 122.1 (CH), 121.0 (CH), 118.7 (CH), 117.0 (CH), 115.9 (CH), 115.0 (C), 114.6 (CH), 67.8 (CH₂), 67.7 (CH₂), 46.7 (CH₃), 30.4 (CH₃), 28.8 (CH₂), 28.6 (CH₂), 28.5 (CH₂), 25.4 (CH₂), 25.4 (CH₂). MS (ESI+): m/z 504.9 [M-2I]²⁺

4.2 Biology

4.2.a. Cell culture

(ISCN cell lines) HT-29 cell line was obtained from ATCC® (HTB-38). Media and complements were purchased from Sigma-aldrich®. Cells were regularly tested for absence of *Mycoplasma*. HT-29 cells were cultured in McCoy (M9309) media, supplemented with 10% Fetal Bovine Serum (FBS), 2 mM L-glutamine and 10,000 units/mL of penicillin and streptomycin. All cell lines have been maintained in humidified incubator supplied with 5% CO₂ at 37 °C. The cells were split twice a week with a ratio from 1:6 to 1:10. For all experiments, cells were seeding between the 2nd and the 20th split, when they were in exponential growth in such a way as to controls never reached confluency.

4.2.b. MTT assay

Formazan powder (M5655) was purchased from Sigma-aldrich (St. Quentin Fallavier, France). Formazan powder was diluted at 5 mg/mL in water and 0.22 μm filtered. Cell viability was determined by MTT according to the manufacturer's instructions. Briefly, 2,500 cells per well were seeded in 96-well plates, and treated 24 h later. Each culture condition was analysed in 4 replicates and the experiment was repeated at least three times. After 72 hours of treatment, 20 μL of the formazan solution were added to each well, and incubated for 2 hours. Then, for each well, the medium was removed and replaced by 200 μL of DMSO. Absorbance values (at 570 nm) were corrected by subtracting the average absorbance from blank wells containing DMSO and the products tested without cells. The absorbance recorded with non-treated cells was taken as 100% of metabolic activity corresponding to the maximum of viability.

4.2.c. Trypan Blue exclusion.

Trypan blue (T8154) was purchased from Sigma-aldrich (St. Quentin Fallavier, France). Cell proliferation was also determined by counting viable and dead cells by Trypan blue exclusion. Cells were seeded in 6-well plates (30,000 cells per well) and treated 24 h after. Each sample was washed by PBS, trypsinized, and then resuspended into media and

diluted with Trypan Blue in a 1:1 ratio. Cells were then counted by optical microscopy (Kova's slide). Each culture condition was analysed 3 times.

4.2.d. Western Blotting

RIPA buffer (R0278), protease inhibitor cocktail (P8349) were purchased from Sigma-aldrich (St. Quentin Fallavier, France). Pierce™ BCA protein assay (23227) were purchased from ThermoFisher Scientific (Life Technologies SAS, Courtabœuf, France). Laemmli buffer (1610737), β-Mercaptoethanol (1610710), 4–15% Mini-PROTEAN® TGX Stain-Free™ Protein Gels (4568084), PVDF-low fluorescence membrane (1620260), Tween-20 (1662404), Clarity Western ECL Substrate (1705060) and all buffers were purchased from Bio-Rad (Bio-Rad Laboratories, Inc, Marnes-la-Coquette, France) or Euromedex. The primary antibodies are listed in Table. Secondary antibodies were purchased from Southern Biotech (Clinisciences).

| Target | Clone and reference | species | dilution |
|---------------|----------------------------------|---------|----------|
| TRAP-1 | 42/Hsp75, BDpharmingen (612344) | Mouse | 1:1000 |
| HSF-1 | 10H8, Enzo life (ADISPA-550D) | Rat | 1:500 |
| Hsp27 | C-20, Santa-Cruz (sc1048) | Goat | 1:500 |
| SDH-A | D-4, Santa-Cruz (sc166947) | Mouse | 1:500 |
| SDH-B | Polyclonal, GeneTex (GTX113833) | Rabbit | 1:250 |

Frozen cell pellets were lysed in RIPA buffer supplemented with protease inhibitor cocktail (10:100) for 30 min on ice (100 µL for 10⁶ cells). Protein concentrations in lysates were assayed using BCA protein assay and 30 µg of proteins were boiled at 95°C for 10 min in presence of Laemmli buffer containing β-Mercaptoethanol (v:v). SDS-PAGE was performed using stain-free precast gels 4-15% (150 V for 1 h). Proteins were then transferred to a PVDF-low fluorescence membrane (100 V for 40 min). The transfer was checked thanks to the stain free technology: upon UV light activation, trihalo compounds are covalently bound to tryptophan residues in order to enhance their fluorescence; thus, enabling total protein loading visualization. For immunodetection, membranes were saturated in 5% non-fat milk in TBS-Tween 0.05% for one hour at room temperature under agitation, and then were incubated with primary antibody dilutions overnight at 4 °C. After washing (3x10 min), horse-radish peroxidase-coupled secondary antibodies were added for 1h and then washed. Detection was achieved using the Clarity Western ECL Substrate. Chemiluminescent signals were analysed using the Chemidoc system (Bio-rad®, France) and were normalized to stain free volumes by the Imagelab software (Bio-rad(r)).

4.2.e. Measurement of mitochondrial membrane potential

Mitochondrial membrane potential was measured by Mitochondrial Membrane Potential Assay Kit (13296) purchased from Cell Signalling and according to manufacturer's instructions. In short, cells were seeded the day before the experiment in black 96-well flat bottom clear plates (2,500 cells per well), and incubated with 6-BrCaQ-C₁₀-TPP at various concentrations for 2, 3 and 6 hours. Each condition was repeated in 3-8 replicates. Some wells were incubated with carbonylcyanure m-chlorophenylhydrazine (CCCP) at 50 µM for positive control of mitochondrial membrane potential disruption for 20 minutes. Then, all the wells were treated with tetramethylrhodamine ethyl ester perchlorate (TMRE) dye at a final concentration of 200 nM for 20 minutes at 37 °C. The plates were then washed 3 times with

warm PBS and then read by fluorescence (ex. 530 nm/em. 590 nm) by Envision Xcite plate reader (PerkinElmer) in the CIBLOT facility (IPSIT, Châtenay-Malabry). The experiment was repeated three times.

5. Acknowledgments

The authors acknowledge support for this project by CNRS, University Paris-Saclay, Ecole Normale Supérieure and Ligue contre le cancer-Comité des Hauts de Seine (2019, 2020). Authors would like to thank Delphine Courilleau for her help to acquire fluorescent data and Magali Noiray for performing the preliminary TSA experiments.

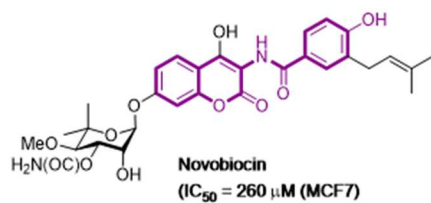
6. References

- (1) Schopf, F. H.; Biebl, M. M.; Buchner, J. The HSP90 Chaperone Machinery. *Nat. Rev. Mol. Cell Biol.* **2017**, *18* (6), 345–360. <https://doi.org/10.1038/nrm.2017.20>.
- (2) Hoter, A.; El-Sabban, M.; Naim, H. The HSP90 Family: Structure, Regulation, Function, and Implications in Health and Disease. *Int. J. Mol. Sci.* **2018**, *19* (9), 2560. <https://doi.org/10.3390/ijms19092560>.
- (3) Patsavoudi, K. S. and E. HSP90 Inhibitors: Current Development and Potential in Cancer Therapy. *Recent Patents Anticancer Drug Discov.* **2013**, *9* (1), 1–20. <https://doi.org/10.2174/15748928113089990031>.
- (4) Solárová, Z.; Mojžiš, J.; Solár, P. Hsp90 Inhibitor as a Sensitizer of Cancer Cells to Different Therapies (Review). *Int. J. Oncol.* **2015**, *46* (3), 907–926. <https://doi.org/10.3892/ijo.2014.2791>.
- (5) Sauvage, F.; Messaoudi, S.; Fattal, E.; Barratt, G.; Vergnaud-Gauduchon, J. Heat Shock Proteins and Cancer: How Can Nanomedicine Be Harnessed? *J. Controlled Release* **2017**, *248*, 133–143. <https://doi.org/10.1016/j.jconrel.2017.01.013>.
- (6) Li, L.; Wang, L.; You, Q.-D.; Xu, X.-L. Heat Shock Protein 90 Inhibitors: An Update on Achievements, Challenges, and Future Directions. *J. Med. Chem.* **2019**, acs.jmedchem.9b00940. <https://doi.org/10.1021/acs.jmedchem.9b00940>.
- (7) Koay, Y. C.; McConnell, J. R.; Wang, Y.; Kim, S. J.; Buckton, L. K.; Mansour, F.; McAlpine, S. R. Chemically Accessible Hsp90 Inhibitor That Does Not Induce a Heat Shock Response. *ACS Med. Chem. Lett.* **2014**, *5* (7), 771–776. <https://doi.org/10.1021/ml500114p>.
- (8) Matts, R. L.; Dixit, A.; Peterson, L. B.; Sun, L.; Voruganti, S.; Kalyanaraman, P.; Hartson, S. D.; Verkhivker, G. M.; Blagg, B. S. J. Elucidation of the Hsp90 C-Terminal Inhibitor Binding Site. *ACS Chem. Biol.* **2011**, *6* (8), 800–807. <https://doi.org/10.1021/cb200052x>.
- (9) Zhang, Z.; You, Z.; Dobrowsky, R. T.; Blagg, B. S. J. Synthesis and Evaluation of a Ring-Constrained Hsp90 C-Terminal Inhibitor That Exhibits Neuroprotective Activity. *Bioorg. Med. Chem. Lett.* **2018**, *28* (16), 2701–2704. <https://doi.org/10.1016/j.bmcl.2018.03.071>.
- (10) Terracciano, S.; Russo, A.; Chini, M. G.; Vaccaro, M. C.; Potenza, M.; Vassallo, A.; Riccio, R.; Bifulco, G.; Bruno, I. Discovery of New Molecular Entities Able to Strongly Interfere with Hsp90 C-Terminal Domain. *Sci. Rep.* **2018**, *8* (1), 1709. <https://doi.org/10.1038/s41598-017-14902-y>.
- (11) Hyun, S. Y.; Le, H. T.; Nguyen, C.-T.; Yong, Y.-S.; Boo, H.-J.; Lee, H. J.; Lee, J.-S.; Min, H.-Y.; Ann, J.; Chen, J.; Park, H.-J.; Lee, J.; Lee, H.-Y. Development of a Novel Hsp90 Inhibitor NCT-50 as a Potential Anticancer Agent for the Treatment of Non-Small Cell Lung Cancer. *Sci. Rep.* **2018**, *8* (1), 13924. <https://doi.org/10.1038/s41598-018-32196-6>.
- (12) Wang, Y.; McAlpine, S. R. N-Terminal and C-Terminal Modulation of Hsp90 Produce Dissimilar Phenotypes. *Chem. Commun.* **2015**, *51* (8), 1410–1413. <https://doi.org/10.1039/C4CC07284G>.
- (13) Sauvage, F.; Fattal, E.; Al-Shaer, W.; Denis, S.; Brotin, E.; Denoyelle, C.; Blanc-Fournier, C.; Toussaint, B.; Messaoudi, S.; Alami, M.; Barratt, G.; Vergnaud-Gauduchon, J. Antitumor Activity of Nanoliposomes Encapsulating the Novobiocin Analog 6BrCaQ in a Triple-Negative Breast Cancer Model in Mice. *Cancer Lett.* **2018**, *432*, 103–111. <https://doi.org/10.1016/j.canlet.2018.06.001>.
- (14) Audisio, D.; Methy-Gonnot, D.; Radanyi, C.; Renoir, J.-M.; Denis, S.; Sauvage, F.; Vergnaud-Gauduchon, J.; Brion, J.-D.; Messaoudi, S.; Alami, M. Synthesis and Antiproliferative Activity of Novobiocin Analogues as Potential Hsp90 Inhibitors. *Eur. J. Med. Chem.* **2014**, *83*, 498–507. <https://doi.org/10.1016/j.ejmech.2014.06.067>.
- (15) Audisio, D.; Messaoudi, S.; Cegielski, L.; Peyrat, J.-F.; Brion, J.-D.; Methy-Gonnot, D.; Radanyi, C.; Renoir, J.-M.; Alami, M. Discovery and Biological Activity of 6BrCaQ as an Inhibitor

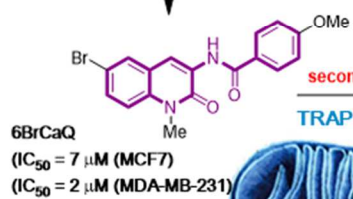
- of the Hsp90 Protein Folding Machinery. *ChemMedChem* **2011**, *6* (5), 804–815. <https://doi.org/10.1002/cmdc.201000489>.
- (16) Sauvage, F.; Franzè, S.; Bruneau, A.; Alami, M.; Denis, S.; Nicolas, V.; Lesieur, S.; Legrand, F.-X.; Barratt, G.; Messaoudi, S.; Vergnaud-Gauduchon, J. Formulation and in Vitro Efficacy of Liposomes Containing the Hsp90 Inhibitor 6BrCaQ in Prostate Cancer Cells. *Int. J. Pharm.* **2016**, *499* (1), 101–109. <https://doi.org/10.1016/j.ijpharm.2015.12.053>.
 - (17) Que, N. L. S.; Crowley, V. M.; Duerfeldt, A. S.; Zhao, J.; Kent, C. N.; Blagg, B. S. J.; Gewirth, D. T. Structure Based Design of a Grp94-Selective Inhibitor: Exploiting a Key Residue in Grp94 To Optimize Paralog-Selective Binding. *J. Med. Chem.* **2018**, *61* (7), 2793–2805. <https://doi.org/10.1021/acs.jmedchem.7b01608>.
 - (18) Park, H.-K.; Jeong, H.; Ko, E.; Lee, G.; Lee, J.-E.; Lee, S. K.; Lee, A.-J.; Im, J. Y.; Hu, S.; Kim, S. H.; Lee, J. H.; Lee, C.; Kang, S.; Kang, B. H. Paralog Specificity Determines Subcellular Distribution, Action Mechanism, and Anticancer Activity of TRAP1 Inhibitors. *J. Med. Chem.* **2017**, *60* (17), 7569–7578. <https://doi.org/10.1021/acs.jmedchem.7b00978>.
 - (19) Hou, X.-S.; Wang, H.-S.; Mugaka, B. P.; Yang, G.-J.; Ding, Y. Mitochondria: Promising Organelle Targets for Cancer Diagnosis and Treatment. *Biomater. Sci.* **2018**. <https://doi.org/10.1039/C8BM00673C>.
 - (20) Porporato, P. E.; Filigheddu, N.; Pedro, J. M. B.-S.; Kroemer, G.; Galluzzi, L. Mitochondrial Metabolism and Cancer. *Cell Res.* **2018**, *28* (3), 265–280. <https://doi.org/10.1038/cr.2017.155>.
 - (21) Battogtokh, G.; Choi, Y. S.; Kang, D. S.; Park, S. J.; Shim, M. S.; Huh, K. M.; Cho, Y.-Y.; Lee, J. Y.; Lee, H. S.; Kang, H. C. Mitochondria-Targeting Drug Conjugates for Cytotoxic, Anti-Oxidizing and Sensing Purposes: Current Strategies and Future Perspectives. *Acta Pharm. Sin. B* **2018**, *8* (6), 862–880. <https://doi.org/10.1016/j.apsb.2018.05.006>.
 - (22) Zielonka, J.; Joseph, J.; Sikora, A.; Hardy, M.; Ouari, O.; Vasquez-Vivar, J.; Cheng, G.; Lopez, M.; Kalyanaraman, B. Mitochondria-Targeted Triphenylphosphonium-Based Compounds: Syntheses, Mechanisms of Action, and Therapeutic and Diagnostic Applications. *Chem. Rev.* **2017**, *117* (15), 10043–10120. <https://doi.org/10.1021/acs.chemrev.7b00042>.
 - (23) Kalyanaraman, B.; Cheng, G.; Hardy, M.; Ouari, O.; Lopez, M.; Joseph, J.; Zielonka, J.; Dwinell, M. B. A Review of the Basics of Mitochondrial Bioenergetics, Metabolism, and Related Signaling Pathways in Cancer Cells: Therapeutic Targeting of Tumor Mitochondria with Lipophilic Cationic Compounds. *Redox Biol.* **2018**, *14*, 316–327. <https://doi.org/10.1016/j.redox.2017.09.020>.
 - (24) Kang, B. H.; Plescia, J.; Song, H. Y.; Meli, M.; Colombo, G.; Beebe, K.; Scroggins, B.; Neckers, L.; Altieri, D. C. Combinatorial Drug Design Targeting Multiple Cancer Signaling Networks Controlled by Mitochondrial Hsp90. *J. Clin. Invest.* **2009**, *119* (3), 454–464. <https://doi.org/10.1172/JCI37613>.
 - (25) Baruchello, R.; Simoni, D.; Grisolia, G.; Barbato, G.; Marchetti, P.; Rondanin, R.; Mangiola, S.; Giannini, G.; Brunetti, T.; Alloatti, D.; Gallo, G.; Ciacchi, A.; Vesci, L.; Castorina, M.; Milazzo, F. M.; Cervoni, M. L.; Guglielmi, M. B.; Barbarino, M.; Foderà, R.; Pisano, C.; Cabri, W. Novel 3,4-Isoxazolidiamides as Potent Inhibitors of Chaperone Heat Shock Protein 90. *J. Med. Chem.* **2011**, *54* (24), 8592–8604. <https://doi.org/10.1021/jm201155e>.
 - (26) Thomas, A. P.; Lee, A.-J.; Palanikumar, L.; Jana, B.; Kim, K.; Kim, S.; Ok, H.; Seol, J.; Kim, D.; Kang, B. H.; Ryu, J.-H. Mitochondrial Heat Shock Protein-Guided Photodynamic Therapy. *Chem. Commun.* **2019**, *55* (84), 12631–12634. <https://doi.org/10.1039/C9CC06411G>.
 - (27) Ross, M. F.; Prime, T. A.; Abakumova, I.; James, A. M.; Porteous, C. M.; Smith, R. A. J.; Murphy, M. P. Rapid and Extensive Uptake and Activation of Hydrophobic Triphenylphosphonium Cations within Cells. *Biochem. J.* **2008**, *411* (3), 633–645. <https://doi.org/10.1042/BJ20080063>.
 - (28) Kalyanaraman, B.; Cheng, G.; Hardy, M.; Ouari, O.; Sikora, A.; Zielonka, J.; Dwinell, M. Mitochondria-Targeted Metformins: Anti-Tumour and Redox Signalling Mechanisms. *Interface Focus* **2017**, *7* (2), 20160109. <https://doi.org/10.1098/rsfs.2016.0109>.
 - (29) Yoo, S. H.; Yoo, S. H.; Kim, H. Y.; Kim, H. Y.; Rho, J. H.; Rho, J. H.; Jeong, S.-Y.; Jeong, S.-Y.; Yun, J.; Yun, J.; Yun, I.; Yun, I.; Park, H. T.; Park, H. T.; Yoo, Y. H.; Yoo, Y. H. Targeted Inhibition of Mitochondrial Hsp90 Induces Mitochondrial Elongation in Hep3B Hepatocellular Carcinoma Cells Undergoing Apoptosis by Increasing the ROS Level. *Int. J. Oncol.* **2015**, *47* (5), 1783–1792. <https://doi.org/10.3892/ijo.2015.3150>.

- (30) Lyamzaev, K. G.; Tokarchuk, A. V.; Panteleeva, A. A.; Mulkidjanian, A. Y.; Skulachev, V. P.; Chernyak, B. V. Induction of Autophagy by Depolarization of Mitochondria. *Autophagy* **2018**, *14* (5), 921–924. <https://doi.org/10.1080/15548627.2018.1436937>.
- (31) Berridge, M. V.; Tan, A. S. Characterization of the Cellular Reduction of 3-(4,5-Dimethylthiazol-2-Yl)-2,5-Diphenyltetrazolium Bromide (MTT): Subcellular Localization, Substrate Dependence, and Involvement of Mitochondrial Electron Transport in MTT Reduction. *Arch. Biochem. Biophys.* **1993**, *303* (2), 474–482. <https://doi.org/10.1006/abbi.1993.1311>.
- (32) Agorreta, J.; Hu, J.; Liu, D.; Delia, D.; Turley, H.; Ferguson, D. J.; Iborra, F.; Pajares, M. J.; Larrayoz, M.; Zudaire, I.; Pio, R.; Montuenga, L. M.; Harris, A. L.; Gatter, K.; Pezzella, F. TRAP1 Regulates Proliferation, Mitochondrial Function, and Has Prognostic Significance in NSCLC. *Mol. Cancer Res.* **2014**, *12* (5), 660–669. <https://doi.org/10.1158/1541-7786.MCR-13-0481>.
- (33) Palladino, G.; Notarangelo, T.; Pannone, G.; Piscazzi, A.; Lamacchia, O.; Sisinni, L.; Spagnoletti, G.; Toti, P.; Santoro, A.; Storto, G.; Bufo, P.; Cignarelli, M.; Esposito, F.; Landriscina, M. TRAP1 Regulates Cell Cycle and Apoptosis in Thyroid Carcinoma Cells. *Endocr. Relat. Cancer* **2016**, *23* (9), 699–709. <https://doi.org/10.1530/ERC-16-0063>.
- (34) Condelli, V.; Piscazzi, A.; Sisinni, L.; Matassa, D. S.; Maddalena, F.; Lettini, G.; Simeon, V.; Palladino, G.; Amoroso, M. R.; Trino, S.; Esposito, F.; Landriscina, M. TRAP1 Is Involved in BRAF Regulation and Downstream Attenuation of ERK Phosphorylation and Cell-Cycle Progression: A Novel Target for BRAF-Mutated Colorectal Tumors. *Cancer Res.* **2014**, *74* (22), 6693–6704. <https://doi.org/10.1158/0008-5472.CAN-14-1331>.
- (35) Zorova, L. D.; Popkov, V. A.; Plotnikov, E. Y.; Silachev, D. N.; Pevzner, I. B.; Jankauskas, S. S.; Babenko, V. A.; Zorov, S. D.; Balakireva, A. V.; Juhaszova, M.; Sollott, S. J.; Zorov, D. B. Mitochondrial Membrane Potential. *Anal. Biochem.* **2018**, *552*, 50–59. <https://doi.org/10.1016/j.ab.2017.07.009>.
- (36) Montague, C. R.; Fitzmaurice, A.; Hover, B. M.; Salazar, N. A.; Fey, J. P. Screen for Small Molecules Increasing the Mitochondrial Membrane Potential. *J. Biomol. Screen.* **2014**, *19* (3), 387–398. <https://doi.org/10.1177/1087057113495295>.
- (37) Goode, K. M.; Petrov, D. P.; Vickman, R. E.; Crist, S. A.; Pascuzzi, P. E.; Ratliff, T. L.; Davisson, V. J.; Hazbun, T. R. Targeting the Hsp90 C-Terminal Domain to Induce Allosteric Inhibition and Selective Client Downregulation. *Biochim. Biophys. Acta Gen. Subj.* **2017**, *1861* (8), 1992–2006. <https://doi.org/10.1016/j.bbagen.2017.05.006>.
- (38) Song, Seon Beom; Jang, So-Young; Kang, Hyun Tae; Wei, Bie; Jeoun, Un-woo; Yoon, Gye Soon; Hwang, Eun Seong. Modulation of Mitochondrial Membrane Potential and ROS Generation by Nicotinamide in a Manner Independent of SIRT1 and Mitophagy. *Mol. Cells* **2017**, *40* (7), 503–514. <https://doi.org/10.14348/MOLCELLS.2017.0081>.
- (39) Papathanassiou, A. E.; MacDonald, N. J.; Bencsura, A.; Vu, H. A. F1F0-ATP Synthase Functions as a Co-Chaperone of Hsp90–Substrate Protein Complexes. *Biochem. Biophys. Res. Commun.* **2006**, *345* (1), 419–429. <https://doi.org/10.1016/j.bbrc.2006.04.104>.
- (40) Hall, J. A.; Kusuma, B. R.; Brandt, G. E. L.; Blagg, B. S. J. Cruentaren A Binds F₁F₀ ATP Synthase To Modulate the Hsp90 Protein Folding Machinery. *ACS Chem. Biol.* **2014**, *9* (4), 976–985. <https://doi.org/10.1021/cb400906e>.
- (41) Margineantu, D. H.; Emerson, C. B.; Diaz, D.; Hockenbery, D. M. Hsp90 Inhibition Decreases Mitochondrial Protein Turnover. *PLoS ONE* **2007**, *2* (10), e1066. <https://doi.org/10.1371/journal.pone.0001066>.
- (42) Chennoufi, R.; Bougherara, H.; Gagey-Eilstein, N.; Dumat, B.; Henry, E.; Subra, F.; Mahuteau-Betzer, F.; Tauc, P.; Teulade-Fichou, M.-P.; Deprez, E. Differential Behaviour of Cationic Triphenylamine Derivatives in Fixed and Living Cells: Triggering and Imaging Cell Death. *Chem. Commun. Camb. Engl.* **2015**, *51* (80), 14881–14884. <https://doi.org/10.1039/c5cc05970d>.
- (43) Hammerer, F.; Poyer, F.; Fourmois, L.; Chen, S.; Garcia, G.; Teulade-Fichou, M.-P.; Maillard, P.; Mahuteau-Betzer, F. Mitochondria-Targeted Cationic Porphyrin-Triphenylamine Hybrids for Enhanced Two-Photon Photodynamic Therapy. *Bioorg. Med. Chem.* **2018**, *26* (1), 107–118. <https://doi.org/10.1016/j.bmc.2017.11.024>.
- (44) Masgras, I.; Sanchez-Martin, C.; Colombo, G.; Rasola, A. The Chaperone TRAP1 As a Modulator of the Mitochondrial Adaptations in Cancer Cells. *Front. Oncol.* **2017**, *7*, 58. <https://doi.org/10.3389/fonc.2017.00058>.

- (45) Matassa, D.; Agliarulo, I.; Avolio, R.; Landriscina, M.; Esposito, F.; Matassa, D. S.; Agliarulo, I.; Avolio, R.; Landriscina, M.; Esposito, F. TRAP1 Regulation of Cancer Metabolism: Dual Role as Oncogene or Tumor Suppressor. *Genes* **2018**, *9* (4), 195. <https://doi.org/10.3390/genes9040195>.
- (46) Sciacovelli, M.; Guzzo, G.; Morello, V.; Frezza, C.; Zheng, L.; Nannini, N.; Calabrese, F.; Laudiero, G.; Esposito, F.; Landriscina, M.; Defilippi, P.; Bernardi, P.; Rasola, A. The Mitochondrial Chaperone TRAP1 Promotes Neoplastic Growth by Inhibiting Succinate Dehydrogenase. *Cell Metab.* **2013**, *17* (6), 988–999. <https://doi.org/10.1016/j.cmet.2013.04.019>.
- (47) Chae, Y. C.; Angelin, A.; Lisanti, S.; Kossenkova, A. A.; Speicher, K. D.; Wang, H.; Powers, J. F.; Tischler, A. S.; Pacak, K.; Fliesner, S.; Michalek, R. D.; Karoly, E. D.; Wallace, D. C.; Languino, L. R.; Speicher, D. W.; Altieri, D. C. LANDSCAPE OF THE MITOCHONDRIAL Hsp90 METABOLOME IN TUMORS. *Nat. Commun.* **2013**, *4*, 2139. <https://doi.org/10.1038/ncomms3139>.
- (48) Kang, B. H.; Plescia, J.; Song, H. Y.; Meli, M.; Colombo, G.; Beebe, K.; Scroggins, B.; Neckers, L.; Altieri, D. C. Combinatorial Drug Design Targeting Multiple Cancer Signaling Networks Controlled by Mitochondrial Hsp90. *J. Clin. Invest.* **2009**, *119* (3), 454–464. <https://doi.org/10.1172/JCI37613>.



first SAR

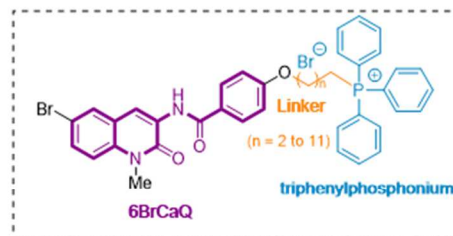


second SAR

TRAP1 targeting



Mitochondrial TRAP1



$n = 9$:

$(IC_{50} = 0.036 \mu M \text{ (HCT-116)})$

$(IC_{50} = 0.107 \mu M \text{ (K562)})$

$(IC_{50} = 0.008 \mu M \text{ (MDA-MB-231)})$

$(IC_{50} = 0.3 \mu M \text{ (PC3)})$